nagra.

Technical Report 19-04

Application of the Bottom-up Approach for the Sorption of Cs(I), Co(II), Ni(II), Eu(III), Th(IV) and U(VI) onto Sedimentary Rocks

December 2021

National Cooperative
for the Disposal of
Radioactive Waste

Hardstrasse 73
CH-5430 Wettingen
Switzerland
Tel. +41 56 437 11 11

www.nagra.ch

nagra.

Technical Report 19-04

Application of the Bottom-up Approach for the Sorption of Cs(I), Co(II), Ni(II), Eu(III), Th(IV) and U(VI) onto Sedimentary Rocks

December 2021

M. Marques Fernandes & B. Baeyens

Paul Scherrer Institut, PSI, Switzerland

National Cooperative
for the Disposal of
Radioactive Waste

Hardstrasse 73
CH-5430 Wettingen
Switzerland
Tel. +41 56 437 11 11

www.nagra.ch

ISSN 1015-2636

Abstract

The safety assessment for the general licence application in the framework of the Swiss Sectoral Plan for Deep Geological Repositories will require a state-of-the-art sorption database. It is foreseen to apply a simplified component additive approach, the so-called bottom-up approach, for the development of the sorption database. This approach allows to calculate directly the solid-liquid distribution ratios (K_d values) for radionuclides by considering aqueous speciation, solubility and concentration-dependent adsorption for site-specific argillaceous rock-porewater systems. Therefore, testing this approach is of key importance to verify its robustness and validate its applicability.

The sorption of radionuclides in natural multi-mineral environments such as geological rock formations is by nature too complex to be easily predicted. The bottom-up approach assumes that in the case of clay-rich environments, retention is controlled by adsorption onto 2:1 clay minerals (e.g. montmorillonite, illite, or illite/smectite mixed layers). In this report, the predictive capability of two in-house adsorption models developed for illite, i.e., the generalised Cs sorption model and the 2 site protolysis non electrostatic surface complexation and cation exchange model, are assessed on realistic geochemical systems. This is achieved by blind predicting adsorption isotherms of Cs(I), Ni(II), Co(II), Eu(III), Th(IV) and U(VI) measured on different rocks (with different clay mineral contents) with the appropriate sorption model, scaled to the 2:1 clay mineral or illite content and by considering the aqueous speciation of the element in the respective porewater. In this approach the sorption model on illite is considered to be also representative for the illite/smectite mixed layers.

In view of the uncertainties related to the complexity of the natural rocks and to the thermodynamic sorption modelling, it can be concluded that the outcome of this modelling exercise is quite satisfying. For Cs(I) and Th(IV), experimental isotherms are very well re-produced. The Eu(III) sorption isotherms for almost all rocks are systematically slightly underestimated, even so the general prediction is rather good. The formation of ternary Eu-carbonate surface complexes, not considered in the modelling, and/or additional partitioning of Eu(III) into calcite might be responsible for the enhanced sorption. In the case of U(VI), the blind predictions are mostly good except for the carbonate-rich Helvetic Marl for which sorption is overpredicted. Aqueous U(VI) carbonate complexes, particularly the non-sorbing ternary uranyl-calcium-carbonate complexes, strongly reduce the sorption of U(VI).

The maximum deviation between blind prediction and experimental data is observed for the divalent transition metals Co and Ni. In the higher equilibrium concentration range of the isotherms, the calculations clearly underestimate the sorption for both metals on most rock samples. The reason for this discrepancy is likely the formation of Ni/Co surface precipitates, not considered in the sorption model since it is not an adsorption mechanism. For the application of the approach in a safety assessment, processes leading to an enhanced uptake of divalent transition metals would be beneficial; however, such high radionuclide releases are not anticipated in the far field of a deep geological repository for radioactive waste. A major contribution of calcite in the retention of divalent cations cannot be confirmed based on this study; however, it is known that divalent transition elements are strongly partionned into calcite.

This study demonstrates that the simplified bottom-up approach provides a fairly good methodology for the adsorption of a number of metals and their appropriate chemical analogues, with oxidation states from I to IV and VI, on clay-rich rocks. For the majority of relevant radionuclides to be considered in a safety assessment, this approach can therefore be applied. In the case where the blind prediction underestimates the observed sorption data (*e.g.* divalent transition metals at high equilibrium concentrations, or in the case of Eu), the bottom-up approach will calculate conservative K_d values for the safety assessment. On the other hand, for the few cases found in this study where the blind prediction overestimates the measurements, the lower limit uncertainty values can be regarded as reliable, as shown in this study. In clay-poor rocks, other minerals, especially calcite, might (partly) control the retention of given metals. If calcite is the dominant mineral in certain sedimentary rocks, a sorption database for calcite has to be applied.

Zusammenfassung

Die Sicherheitsbeurteilung für das Rahmenbewilligungsgesuch im Rahmen des Sachplans geologische Tiefenlager der Schweiz erfordert eine Sorptionsdatenbank nach dem neusten Stand der Technik. Für die Entwicklung der Sorptionsdatenbank ist ein vereinfachter, komponentenadditiver Ansatz, der sogenannte Bottom-up-Ansatz, vorgesehen. Dieser ermöglicht die direkte Berechnung der Fest-Flüssig-Verteilungsverhältnisse (K_d-Werte) für Radionuklide unter Berücksichtigung der wässrigen Speziation, der Löslichkeit und der konzentrationsabhängigen Adsorption für standortspezifische Tongestein-Porenwasser-Systeme. Die Erprobung dieses Ansatzes auf Robustheit und Anwendbarkeit ist daher von entscheidender Bedeutung.

Die Sorption von Radionukliden in natürlichen multimineralischen Umgebungen wie z. B. geologischen Gesteinsformationen ist von Natur aus zu komplex, um leicht vorhergesagt werden zu können. Der Bottom-up-Ansatz geht davon aus, dass in tonreichen Umgebungen die Rückhaltung von Radionukliden durch Adsorption an 2:1-Tonmineralien (z. B. Montmorillonit, Illit oder Illit/Smektit-Mischschichten) gesteuert wird. In diesem Bericht wird die Vorhersagefähigkeit von zwei für Illit eigens entwickelten Adsorptionsmodellen getestet. Hierbei wird das verallgemeinerte Cs-Sorptionsmodell und das "zwei Platz Protolyse nicht elektrostatische Oberflächenkomplexierungs- und Kationenaustausch-Modell" an realistischen geochemischen Systemen angewendet. Dabei werden Adsorptionsisothermen von Cs(I), Ni(II), Co(II), Eu(III), Th(IV) und U(VI), skaliert auf den 2:1-Tonmineral- oder Illitgehalt und unter Berücksichtigung der wässrigen Speziation des Elements im jeweiligen Porenwasser, theoretisch berechnet. Bei diesem Ansatz wird davon ausgegangen, dass das Sorptionsmodell für Illit auch für Illit/Smektit-Mischschichten repräsentativ ist.

In Anbetracht der Ungewissheiten, die mit der Komplexität der natürlichen Gesteine und der thermodynamischen Sorptionsmodellierung zusammenhängen, sind die Ergebnisse dieser Modellierung recht zufriedenstellend. Für Cs(I) und Th(IV) werden die experimentellen Isothermen sehr gut reproduziert. Die Sorptionsisothermen für Eu(III) sind für fast alle Gesteine systematisch leicht unterschätzt, wobei die allgemeine Vorhersage recht gut ist. Die Bildung von ternären Eu-Karbonat-Oberflächenkomplexen, die in der Modellierung nicht berücksichtigt wurden, und/oder eine zusätzliche Ausfällung von Eu(III) in Calcit könnten für die erhöhte Sorption verantwortlich sein. Im Falle von U(VI) sind die Vorhersagen recht gut, ausser für den karbonatreichen Helvetischen Mergel, für den die Sorption überschätzt wird. Wässrige U(VI)-Karbonatkomplexe, insbesondere die nicht sorbierenden ternären Uranyl-Kalzium-Karbonat-Komplexe, verringern die Sorption von U(VI) hierbei stark.

Die grösste Abweichung zwischen der Vorhersage und experimentellen Daten wird für die zweiwertigen Übergangsmetalle Co und Ni beobachtet. Für höhere Gleichgewichtskonzentrationen in den Isothermen unterschätzen die Berechnungen die Sorption für beide Metalle in den meisten Gesteinsproben deutlich. Der Grund für diese Diskrepanz ist wahrscheinlich die Bildung von Ni/Co-Oberflächenausfällungen, die im Sorptionsmodell nicht berücksichtigt werden, da es sich nicht um einen Adsorptionsmechanismus handelt. Für die Anwendung des Ansatzes in einer Sicherheitsbeurteilung wären Prozesse, die zu einer verstärkten Aufnahme von zweiwertigen Übergangsmetallen führen, von Vorteil; im Fernfeld eines geologischen Tiefenlagers für radioaktive Abfälle sind derart hohe Radionuklidfreisetzungen jedoch nicht zu erwarten. Ein wesentlicher Beitrag von Calcit zur Rückhaltung von zweiwertigen Kationen kann auf der Grundlage dieser Studie nicht bestätigt werden; es ist jedoch bekannt, dass zweiwertige Übergangselemente vermehrt in Calcit eingelagert werden können.

Diese Studie zeigt, dass der vereinfachte Bottom-up-Ansatz eine recht gute Methodik für die Adsorption einer Reihe von Metallen und ihrer entsprechenden chemischen Analoga mit Oxidationsstufen von I bis IV und VI an tonreichen Gesteinen bietet. Für die Mehrzahl der relevanten Radionuklide, die in einer Sicherheitsbeurteilung zu berücksichtigen sind, kann dieser Ansatz daher angewendet werden. In den Fällen, in denen die Vorhersage die beobachteten Sorptionsdaten unterschätzt (z.B. bei zweiwertigen Übergangsmetallen mit hohen Gleichgewichtskonzentrationen oder Eu), werden mit dem Bottom-up-Ansatz konservative K_d-Werte für die Sicherheitsbeurteilung berechnet. In den wenigen Fällen, in denen die Messungen durch die Vorhersage überschätzt werden, können die Werte der unteren Ungewissheitsgrenze als zuverlässig angesehen werden. In tonarmen Gesteinen können andere Mineralien, insbesondere Calcit, die Rückhaltung von gewissen Metallen beeinflussen. Wenn Calcit das dominierende Mineral in bestimmten Sedimentgesteinen ist, muss dafür eine Sorptionsdatenbank für Calcit verwendet werden.

Résumé

L'évaluation de la sûreté de potentielles sites d'implantation des dépôts en couches géologiques profondes pour la demande d'autorisation générale exige une base de données de sorption thermodynamique selon l'actuel état des connaissances. L'utilisation d'une approche thermodynamique d'addition des composantes simplifiée, appelée approche bottom-up, est envisagée pour le développement de la base de données de sorption. Cette approche permet de calculer directement les coefficients de partage solide-liquide (valeurs K_d) pour les différents radionucléides, en tenant compte de leur spéciation, de leur solubilité et leur concentration (comportement de sorption non-linéaire) pour les différentes eaux interstitielles spécifiques aux sites. Il est donc crucial de vérifier la robustesse et l'applicabilité de cette approche.

La sorption des radionucléides dans des environnements naturels multi-minéraux tels que des formations géologiques est par nature trop complexe pour être facilement prédite. L'approche simplifiée assume que dans les environnements argileux, la rétention des radionucléides est contrôlée par l'adsorption sur les minéraux argileux du type 2:1 (tels que montmorillonite, illite ou interstratifiés illite/smectite). Dans le présent rapport, la capacité de prédiction de deux modèles d'adsorption c.à.d. le "generalised Cs sorption model" et le "2 site protolysis non electrostatic surface complexation and cation exchange model" développés spécifiquement pour l'illite est testée sur des systèmes géochimiques réelles. Pour cela, les isothermes d'adsorption de Cs(I), Ni(II), Co(II), Eu(III), Th(IV) et U(VI) sont calculées théoriquement avec le model adéquat, en fonction de la teneur en minéraux argileux et en tenant compte de la spéciation aqueuse de l'élément dans l'eau interstitielle respective. Cette approche suppose que le modèle de sorption pour l'illite est également représentatif des couches mixtes illite/smectite.

Compte tenu des incertitudes liées à la complexité des roches naturelles et à la modélisation thermodynamique de la sorption, les résultats de cette modélisation sont tout à fait satisfaisants. Pour le Cs(I) et le Th(IV), les isothermes expérimentales sont très bien reproduites. Les isothermes de sorption pour l'Eu(III) sont systématiquement légèrement sous-estimées pour presque toutes les roches, bien que la prédiction générale soit assez bonne. La formation de complexes ternaires de surface Eu-carbonate, qui n'ont pas été pris en compte dans la modélisation, et/ou une précipitation supplémentaire de Eu(III) dans la calcite pourraient être responsables de l'augmentation de la sorption. Dans le cas de l'U(VI), les prédictions sont assez bonnes, sauf pour les marnes helvétiques riches en carbonates, pour lesquelles la sorption est surestimée. Les complexes aqueux de carbonate de U(VI), en particulier les complexes ternaires de carbonate d'uranyle et de calcium non absorbants, réduisent fortement la sorption de U(VI).

La plus grande déviation entre la prédiction et les données expérimentales est observée pour les métaux de transition divalents Co et Ni. Pour des concentrations d'équilibre plus élevées dans les isothermes, les calculs sous-estiment significativement la sorption pour les deux métaux dans la plupart des échantillons de roche. La raison de cette divergence est probablement la formation de précipités de surface Ni/Co, qui ne sont pas pris en compte dans le modèle de sorption car il ne s'agit pas d'un mécanisme d'adsorption. Outre l'applicabilité de l'approche, les processus conduisant à une absorption accrue des métaux de transition divalents seraient bénéfiques; toutefois, des rejets de radionucléides aussi élevés ne sont pas attendus dans le champ lointain d'un dépôt géologique profond pour déchets radioactifs. Une contribution significative de la calcite à la rétention des cations divalents ne peut pas être confirmée sur la base de cette étude; cependant, il est connu que les éléments de transition divalents peuvent être retenu dans la calcite.

Cette étude montre que l'approche bottom-up fournit une méthodologie appropriée pour prédire l'adsorption d'une gamme de métaux et de leurs analogues chimiques avec des états d'oxydation de I à IV et VI dans des roches argileuses et leurs eaux interstitielles correspondantes. Cette approche peut donc être appliquée pour la majorité des radionucléides à prendre en compte dans l'évaluation de la sureté. Dans les cas où la prédiction sous-estime les données de sorption mesurées (par exemple pour les métaux de transition divalents avec des concentrations à l'équilibre élevées ou pour l'Eu(III), l'approche calcule des valeurs K_d conservatrices. Dans les quelques cas où la prédiction surestime les données expérimentales, les valeurs de la limite inférieure d'incertitude peuvent être considérées comme fiables. Dans les roches pauvres en argile, d'autres minéraux, notamment la calcite, peuvent influencer la rétention de certains métaux. Pour les roches où la calcite est le minéral dominant, il faut utiliser une base de données de sorption pour la calcite.

Table of Contents

List of Tables

List of Figures

1 Introduction

In any activity involving the understanding and modelling of the migration of aqueous metal species through geological media, the partitioning of the dissolved species between the aqueous phase and immobile solid surfaces (sorption) is a primary consideration. It is currently common practice to treat the reversible adsorption in terms of a distribution ratio, R_d,

$$R_d = C_{sorb} / C_{eq} \quad (1)$$

In clay-rich soils and rocks, reactions at the solid-liquid interface of clay minerals are of particular importance since they are (in most cases) governing the metal uptake. The focus of the work described in this report is on the 2:1 clay mineral illite in natural rock formations, which are particularly important in the context of radioactive waste disposal in deep geological repositories in Switzerland (Nagra 2002). The approach and methodology to be described are, in principle, applicable to any system involving the migration of aqueous metal species through media containing significant amounts of clay minerals.

The disposal of radioactive waste in deep geological repositories aims at isolating the radionuclides from the biosphere for many hundreds of thousands of years. Sorption is a complex process, and it is therefore rather unsatisfactory that the whole of the complexity of the radionuclide-water-rock interacting system is often contained in a single empirical R_d term. Because of the nature of this approach, extrapolation to other (geochemical) conditions, and particularly to other systems, is highly questionable. Such a purely empirical approach has clear and significant disadvantages in that it lacks predictive capabilities. Therefore, there is a pressing need for a better understanding of adsorption processes of aqueous species and the factors affecting them. This has led to the development of adsorption models based on a mechanistic approach. Consequently, these models have been used to produce adsorption databases for montmorillonite (Baeyens & Bradbury 2017) and illite (Bradbury & Baeyens 2017), containing mineral-specific characteristics such as site types, site capacity values, protolysis constants, selectivity coefficients and surface complexation constants (SCCs), *i.e.*, thermodynamic sorption databases (SDBs).

The overall aim of this report is to test the predictive capability of the simplified component additive (CA) approach, the so-called bottom-up approach, towards adsorption (Bradbury & Baeyens 2011). In general, the predictive CA approach considers all minerals constituting the natural system with their unique adsorption properties, requiring adsorption models for each single mineral component of the assemblage (e.g. Arnold et al. 2001, Davis et al. 1998, OECD/NEA 2012). However, the CA modelling can be substantially simplified when one mineral component is assumed to control adsorption (Payne et al. 2013). In the case of clay-rich environments, 2:1 clay minerals (e.g. montmorillonite, illite, or illite/smectite mixed layers ISML) are assumed to be the preferential sorbing phases (Bradbury & Baeyens 2011, Marques Fernandes et al. 2015). Although all of the necessary information is not fully available, the current knowledge and understanding level should be sufficiently advanced to test the predictive capabilities of this approach on chemically realistic systems, and to assess the extent of its applicability.

This report is a state-of-the-art compilation of already published studies on the bottom-up approach applied to Opalinus Clay (Bradbury & Baeyens 2011), Boom Clay/Oxford Clay/Marl (Bradbury & Baeyens 2000) and Boda Claystone (Marques Fernandes et al. 2015), data sets contained in Baeyens et al. (2014) as well as unpublished in-house data. The layout of the report is structured in chapters by elements (*i.e.*, Cs(I), Ni(II), Co(II), Ni(II), Eu(III), Th(IV) and U(VI)), and by different sedimentary rock formations in the sub-sections within a chapter. The adsorption was blind predicted with two adsorption models developed for illite, namely the generalised Cs(I) sorption (GCS) model (Bradbury & Baeyens 2000) and the 2 Site Protolysis Non Electrostatic Surface Complexation and Cation Exchange (2SPNE SC/CE) model (Bradbury & Baeyens 2009a, 2009b, 2017) and compared to the experimentally obtained data.

For the safety analysis for the general licence application in the framework of the Swiss Sectoral Plan for Deep Geological Repositories (SGT), a state-of-the-art thermodynamic SDB is required. It is foreseen to apply the bottom-up approach for the development of the SDB in that the R_d values will be calculated directly, including aqueous speciation, solubility and concentration-dependent adsorption of the radionuclides for site-specific argillaceous rock/porewater systems. The validation of the bottom-up approach is of key importance to justify its applicability in the framework of an important upcoming safety assessment.

2 Adsorption models for illite

2.1 The 2SPNE SC/CE model

The surfaces of 2:1 clay mineral platelets carry a permanent negative charge arising from isomorphous substitution of lattice cations by cations of a lower valence. Charge neutrality is maintained by the presence of an excess of cations in solution held electrostatically in close proximity around the outside of the Si-Al-Si clay mineral units. The electrostatically bound cations, which constitute the electrical double layer, can undergo stoichiometric exchange with the cations in solution (Grim 1953, Van Olphen 1963). The total permanent negative charge of a clay mineral is defined as the cation exchange capacity (CEC).

A second category of reactive sites associated with clay minerals are surface hydroxyl groups (≡SOH) situated along the edges of the clay platelets, "edge" or "broken bond" sites. These sites protonate and deprotonate as a function of pH and form surface complexes with aqueous metal species.

2:1 clay minerals such as illite and ISML are of importance because of their high reactivity and their ubiquity in argillaceous rocks (see mineralogical compositions in Chapter 3). The adsorption properties of illite were investigated in terms of its protolysis (titration measurements) and retention (adsorption edge and isotherm measurements) behaviour. From these data, a multi-site mass action adsorption model combining protolysis, surface complexation and cation exchange was developed, without an electrostatic term, to quantitatively describe the uptake of aqueous metal species on this clay mineral (Bradbury & Baeyens 2009a, b). The adsorption model originally developed for montmorillonite (Baeyens & Bradbury 1997, Bradbury & Baeyens, 1997) and denoted as the 2SPNE SC/CE model was applied. In order to describe the titration measurements, reactions on two types of weak sites (≡S^{W1}OH and ≡S^{W2}OH) with a similar site capacity were required. To describe metal adsorption edge and isotherm data, also two site types were required, so called strong sites, ≡S^{S}OH type sites, and the ≡S^{W1}OH weak type sites. The ≡S^{S}OH type sites have a much smaller capacity but form considerably stronger surface complexes with metals and dominate the adsorption at trace concentrations. Within the application of the bottom-up approach, we assume that ISML have essentially the same adsorption characteristics as illite. This can be justified by the very similar adsorption characteristics of metals on both clay minerals (see e.g. Baeyens & Marques Fernandes 2018). The model calculations are carried out using the MINSORB code (Bradbury & Baeyens 1997) together with the PSI/Nagra TDB (Thoenen et al. 2014).

A summary of the different site types, site capacities and corresponding protolysis constants for illite are given in Tab. 2-1. It is important to note that the parameters and associated values given are fixed in all modelling calculations, provided later.

A surface complexation reaction used for surface edge binding can be written as:

$$\equiv SOH + ME^{z} + y\,H_sO \Leftrightarrow \equiv SOMe(OH)_y^{z-(y+1)} + (y+1)\,H^1 \quad (3)$$

Where Me is a metal with valence z, and y an integer. For $y = 0$, the surface complex is ≡SOMe$^{(z-1)}$.

In a non-electrostatic model, the corresponding SCC, K_y can be expressed as:

$$K_y = \frac{[\equiv SOMe(OH)_y^{z-(y+1)}]}{[\equiv SOH]} \cdot \frac{\{H\}^{(y+1)}}{\{Me^z\}} \quad (4)$$

Where [ ] terms are concentrations and {} terms are aqueous activities.

The 2SPNE SC/CE model was developed in simple background electrolytes (NaCl/$NaClO_4$) and only free cationic and hydrolysed species are considered to adsorb by surface complexation. The SCCs and selectivity coefficients for the metals compiled in this report are taken from Bradbury & Baeyens (2017) and are summarised in Tabs. 2-2 and 2-3. The SCCs are strongly related to the metal hydrolysis constants, and these data are summarised in Tab. 2-4.

Tab. 2-1: Summary of site types, site capacities and protolysis constants for illite

Bradbury & Baeyens (2009a)

Site type	**Capacity** [mol kg^{-1}]	
$\equiv S^{S}OH$	2.0×10^{-3}	
$\equiv S^{W1}OH$	4.0×10^{-2}	
$\equiv S^{W2}OH$	4.0×10^{-2}	
Protolysis reactions	**log K**	
	$\equiv S^{S/W1}OH$	$\equiv S^{W2}OH$
$\equiv SOH + H^+ \Leftrightarrow \equiv SOH_2^+$	4.0	8.5
$\equiv SOH \Leftrightarrow \equiv SO^- + H^+$	-6.2	-10.5

Tab. 2-2: Surface complexation reactions and constants on strong ($\equiv S^{S}OH$) and weak ($\equiv S^{W1}OH$) sites for the adsorption of Co(II), Ni(II), Eu(III), Th(IV) and U(VI) on Na-illite

Bradbury & Baeyens (2017)

Surface complexation reaction	**log $^{S/W1}K_{SC}$**
$\equiv S^{S}OH + Ni^{2+} \Leftrightarrow \equiv S^{S}ONi^+ + H^+$	0.7
$\equiv S^{S}OH + Ni^{2+} + H_2O \Leftrightarrow \equiv S^{S}ONiOH^0 + 2\ H^+$	-8.2
$\equiv S^{S}OH + Ni^{2+} + 2\ H_2O \Leftrightarrow \equiv S^{S}ONi(OH)_2^- + 3\ H^+$	-17.3
$\equiv S^{W1}OH + Ni^{2+} \Leftrightarrow \equiv S^{W1}ONi^+ + H^+$	-1.8
$\equiv S^{S}OH + Co^{2+} \Leftrightarrow \equiv S^{S}OCo^+ + H^+$	0.9
$\equiv S^{S}OH + Co^{2+} + H_2O \Leftrightarrow \equiv S^{S}OCoOH^0 + 2\ H^+$	-7.0
$\equiv S^{S}OH + Co^{2+} + 2\ H_2O \Leftrightarrow \equiv S^{S}OCo(OH)_2^- + 3\ H^+$	-16.5
$\equiv S^{W1}OH + Co^{2+} \Leftrightarrow \equiv S^{W1}OCo^+ + H^+$	-2.0
$\equiv S^{S}OH + Eu^{3+} \Leftrightarrow \equiv S^{S}OEu^{2+} + H^+$	1.9
$\equiv S^{S}OH + Eu^{3+} + H_2O \Leftrightarrow \equiv S^{S}OEuOH^+ + 2\ H^+$	-4.7
$\equiv S^{S}OH + Eu^{3+} + 2\ H_2O \Leftrightarrow \equiv S^{S}OEu(OH)_2^0 + 3\ H^+$	-12.7
$\equiv S^{W1}OH + Eu^{3+} \Leftrightarrow \equiv S^{W1}OEu^{2+} + H^+$	0.3
$\equiv S^{W1}OH + Eu^{3+} + H_2O \Leftrightarrow \equiv S^{W1}OEuOH^+ + 2\ H^+$	-6.2

Tab. 2-2: continued

Surface complexation reaction	**log $^{S/W1}K_{SC}$**
$\equiv S^{S}OH + UO_2^{2+} \Leftrightarrow \equiv S^{S}OUO_2^{+} + H^{+}$	2.0
$\equiv S^{S}OH + UO_2^{2+} + H_2O \Leftrightarrow \equiv S^{S}OUO_2OH^{0} + 2\ H^{+}$	-3.9
$\equiv S^{S}OH + UO_2^{2+} + 2\ H_2O \Leftrightarrow \equiv S^{S}OUO_2(OH)_2^{-} + 3\ H^{+}$	-10.8
$\equiv S^{S}OH + UO_2^{+2+} + 3\ H_2O \Leftrightarrow \equiv S^{S}OUO_2(OH)_3^{2-} + 4\ H^{+}$	-18.7
$\equiv S^{W1}OH + UO_2^{2+} \Leftrightarrow \equiv S^{W1}OUO_2^{+} + H^{+}$	0.0
$\equiv S^{W1}OH + UO_2^{2+} + H_2O \Leftrightarrow \equiv S^{W1}OUO_2OH^{0} + 2\ H^{+}$	-5.8
$\equiv S^{W1}OH + UO_2^{2+} + 2H_2O \Leftrightarrow \equiv S^{W1}OUO_2OH^{-}{}_2 + 3\ H^{+}$	-12.3

Tab. 2-3: Cation exchange reactions and the corresponding selectivity coefficient values (log K_c) for Co(II), Ni(II), Eu(III) and U(VI) on Na-illite

Bradbury & Baeyens (2017)

Cation exchange reaction	**log K_c**
2 Na-illite + $Co^{2+} \Leftrightarrow$ Co-illite + 2 Na^{+}	1.3
2 Na-illite + $Ni^{2+} \Leftrightarrow$ Ni-illite + 2 Na^{+}	1.1
3 Na-illite + $Eu^{3+} \Leftrightarrow$ Eu-illite + 3 Na^{+}	1.9
2 Na-illite + $UO_2^{2+} \Leftrightarrow$ UO_2-illite + 2 Na^{+}	0.65

Tab. 2-4: Hydrolysis constants (log K values) for Co(II), Ni(II), Eu(III), Th(IV) and U(VI) used in the 2SPNE SC/CE adsorption model

Metal complex	**Co[a]**	**Ni[a]**	**Eu[b]**	**Th[c]**	**U[a]**
$Me^{z} + H_2O \Leftrightarrow Me(OH)^{(z-1)} + H^{+}$	-9.23	-9.54	-7.2	-2.2	-5.25
$Me^{z} + 2\ H_2O \Leftrightarrow Me(OH)_2^{(z-2)} + 2H^{+}$	-18.6	-18	-15.1	-6.0	-12.15
$Me^{z} + 3\ H_2O \Leftrightarrow Me(OH)_3^{(z-3)} + 3H^{+}$	-31.7	-29.2	-26.2	-11.0	-20.25
$Me^{z} + 4\ H_2O \Leftrightarrow Me(OH)_4^{(z-4)} + 4\ H^{+}$	-46.42	-	-	-17.5	-32.4
$2\ Me^{z} + 2\ H_2O \Leftrightarrow Me_2(OH)_2^{(z-1)} + 2\ H^{+}$	-	-	-	-	-5.62
$3\ Me^{z} + 5\ H_2O \Leftrightarrow Me_3(OH)_5^{(3z-5)} + 5\ H^{+}$	-	-	-	-	-15.55
$4\ Me^{z} + 7\ H_2O \Leftrightarrow Me_4(OH)_7^{(4z-7)} + 7\ H^{+}$	-	-	-	-	-21.9

[a, b] Taken from Thoenen et al. (2014), with the stability constants for Eu(III) assumed to be the same as for Am(III)
[c] Taken from Neck & Kim (2001)

Tab. 2-5: Cation exchange site types and their corresponding capacities for Cs(I) on illite

Site type	**Site capacity**
Frayed edge sites (FES)	0.25% of the CEC*
Type II sites (T2S)	20% of the CEC
Planar sites (PS)	~ 80% of the CEC

* CEC = 200 meq kg^{-1}

Tab. 2-6: Selectivity coefficients K_c for the cation exchange equilibria on the three site types of illite for Cs, K, NH_4 and Ca w.r.t. Na on illite with a CEC = 200 meq kg^{-1}

Site type	**FES**	**T2S**	**PS**
Site capacity [meq kg^{-1}]	0.5	40	160
Exchange equilibrium	**log K_c**		
$Cs^+ + Na^+$-illite ⇔ Cs^+-illite + Na^+	7.0	3.6	1.6
$K^+ + Na^+$-illite ⇔ K^+-illite + Na^+	2.4	2.1	1.1
$NH_4^+ + Na^+$-illite ⇔ NH_4^+-illite + Na^+	3.4*	2.1*	0.9*
$Ca^{2+} + 2Na^+$-illite ⇔ Ca^{2+}-illite + $2Na^+$	0.2*	0.0*	0.4*

* Taken from Wick et al. (2018)

2.2 Generalised caesium adsorption model

The GCS model is taken from the work of Bradbury & Baeyens (2000) where a detailed model description can be found. The adsorption of Cs(I) on illite is purely based on cation exchange reactions and is assumed to take place on three different site types, denoted as frayed edge sites (FES), type II sites (T2S) and planar sites (PS), each having a given site capacity and affinity for Cs(I). The relations between these site capacities are expressed in Tab. 2-5 as fixed percentages of the CEC of illite. An integral assumption in the model concept is that the relationship between the three different sites is valid for all illites irrespective of their origin, as shown by Bradbury & Baeyens (2000). It should be noted that FES and T2S are not present in smectites and their presence in soils and sediments can be used as a fingerprint for Cs(I) adsorption onto illite.

Selectivity coefficients for Cs(I) and the main competing cations (K, Ca and NH_4) were converted from experimental adsorption data on illite taken from literature (Brouwer et al. 1983, Wick et al. 2018). The set of "reference selectivity coefficients", considered generally valid for all illite clay minerals and non-adjustable model parameters in the illite model, are listed in Tab. 2-6.

In illite and argillaceous rock systems, at Cs(I) equilibrium concentrations ($[Cs_{eql}]$) < 10^{-3} M, only the Cs uptake on FES and T2S is important. These sites are predominantly accessible to cations with low hydration energies (e.g. K and NH_4) and these cations compete most effectively with Cs. Na may also compete, but only when the concentration is many orders of magnitude greater than that of Cs and/or K or NH_4. Divalent cations such as Mg, Ca and Sr, with relatively large hydration energies, are effectively non-competitive for steric reasons (Brouwer et al. 1983). FES

exhibit the strongest affinity for Cs and are the main sorbing sites at concentrations < 10^{-8} M, where the adsorption is linear. In the concentration range up to ~ 10^{-4} M, T2S dominate and the adsorption is non-linear. Non-linear adsorption behaviour extends to even higher concentrations due to contributions from the planar sites and site saturation effects.

2.3 Predictive modelling: bottom-up approach

To blind predict the retention of the selected elements on sedimentary rocks described in this report, a simplified component additivity or bottom-up approach was chosen. This approach is based on the hypothesis that the uptake of cations in argillaceous rocks is predominantly controlled by adsorption on the major clay mineral components. Quantitative predictions are then possible based on the knowledge and understanding of the mechanistic adsorption processes on these clay minerals, and the models developed to describe them. The 2:1 clay minerals illite and ISML are major components of most investigated rock samples, and their respective contents are given for each rock type considered in this report. The detailed mineralogical compositions are provided in Chapter 3. A further assumption is that ISML have similar adsorption behaviour on the amphoteric edge site as illite. This assumption cannot be confirmed unambiguously because adsorption data for ISML are very sparse in the open literature. However, the similarities in terms of surface complexation behaviour for many cations on illite and montmorillonite are well described in the literature (e.g. Baeyens & Marques Fernandes 2018).

In the present report, the GCS and 2SPNE SC/CE models are used to blind predict adsorption isotherms measured on samples from different rock formations in their corresponding porewaters.

The adsorption of Cs(I) on the rock samples is modelled by scaling the capacity of the cation exchange sites (*i.e.*, FES, T2S and PS) (Tab. 2-5) only to the illite content of the natural rocks according to the GCS model (Bradbury & Baeyens 2000). As mentioned before, FES and T2S are not present in smectites and retention of Cs at trace and medium concentration is solely governed by adsorption on these two sites.

The adsorption was modelled by scaling the capacity of the surface complexation sites of the 2SPNE SC/CE model for illite (Tab. 2-1) to the 2:1 clay mineral content (illite, ISML) of the respective rock sample and by considering the aqueous speciation for each element in the associated porewaters. The applied modelling approach in this study only considers adsorption of each specific element as the uptake mechanism. The potential influence of competing cations like divalent Fe on the adsorption of the divalent metals Ni(II) and Co(II), as shown in a recent study (Marques Fernandes & Baeyens 2020), was not considered in the present modelling exercise. All experiments were set up within experimental conditions (*i.e.*, pH, cation concentrations) in which the precipitation of known solubility limiting phases was avoided. Further, we use "sorption" for the experimental uptake data since we cannot exclude that other uptake processes (even to a small extent) contribute to the retention of any of the investigated elements on the different rock samples and "adsorption" for the modelling.

Tab. 2-7: Summary of the aqueous complexation constants (log K values in) for Co(II), Ni(II), Eu(III), Th(IV) and U(VI) with chloro, sulphato and carbonato species used in the blind prediction calculations

Data from Thoenen et al. (2014)

Metal complex	**Co**	**Ni**	**Eu[a]**	**Th**	**U**
$Me^z + Cl^- \Leftrightarrow MeCl^{(z-1)}$	0.57	0.08	0.24	1.70	0.17
$Me^z + 2\ Cl^- \Leftrightarrow MeCl_2^{(z-2)}$	0.02	-	-0.74	-	-1.1
$Me^z + SO_4^{2-} \Leftrightarrow MeSO_4^{(z-2)}$	2.3	2.35	3.30	6.17	3.15
$Me^z + 2\ SO_4^{2-} \Leftrightarrow Me(SO_4)_2^{(z-4)}$	-	-	3.7	9.69	4.14
$Me^z + 3\ SO_4^{2-} \Leftrightarrow Me(SO_4)_3^{(z-6)}$	-	-	-	10.75	3.02
$Me^z + CO_3^{2-} \Leftrightarrow MeCO_3^{(z-2)}$	4.23	4.2	8.0	-	9.94
$Me^z + 2\ CO_3^{2-} \Leftrightarrow Me(CO_3)_2^{(z-2)}$	6.0	6.0	12.9	-	16.61
$Me^z + 3\ CO_3^{2-} \Leftrightarrow Me(CO_3)_3^{(z-2)}$	-	-	15.0	-	21.84
$Me^z + HCO_3^- \Leftrightarrow MeHCO_3^{(z-1)}$	12.22	11.72	3.1	-	-
$Me^z + 5\ CO_3^{2-} \Leftrightarrow Me(CO_3)_5^{(z-5)}$	-	-	-	31.0	-
$Me^z + 2\ H_2O + 2\ CO_3^{2-} \Leftrightarrow Me(OH)_2(CO_3)_2^{(z-6)}$	-	-	-	8.80	-
$Me^z + H_2O + 4\ CO_3^{2-} \Leftrightarrow Me(OH)(CO_3)_4^{(z-9)}$	-	-	-	21.6	-
$Me^z + 4\ H_2O + CO_3^{2-} \Leftrightarrow Me(OH)_4CO_3^{(z-6)}$	-	-	-	-15.6	-
$Me^z + Mg^{2+} + 3\ CO_3^{2-} \Leftrightarrow MeMg(CO_3)_3^{(z-4)}$	-	-	-	-	26.11
$Me^z + Ca^{2+} + 3\ CO_3^{2-} \Leftrightarrow MeCa(CO_3)_3^{(z-4)}$	-	-	-	-	27.18
$Me^z + 2\ Ca^{2+} + 3\ CO_3^{2-} \Leftrightarrow MeCa_2(CO_3)_3^{(z-2)}$	-	-	-	-	29.22
$2\ Me^z + 3\ H_2O + CO_3^{2-} \Leftrightarrow Me_2(OH)_3CO_3^{(2z-5)}$	-	-	-	-	-0.86

[a] The stability constants for Eu(III) were assumed to be the same as for Am(III).

The aqueous speciation of the considered element plays a very important role in calculating its adsorption values with the 2SPNE SC/CE model. The correctness and completeness of the thermodynamic database used in the calculations are critical. A summary of the thermodynamic aqueous complexation constants used for the speciation calculations is given in Tab. 2-6 (hydrolysis) and Tab. 2-7 (major inorganic ligands). Because of their very close thermodynamic properties, trivalent Eu and Am are often used as chemical analogues (Choppin 1995). For this reason and to be consistent with the SCCs for Eu(III) on illite, Am(III) hydrolysis and Am-chloro, -sulphato and -carbonato complexation constants were used in the calculations. Aqueous activity coefficients were calculated using the Davies relation (Davies 1962). The Co(II), Ni(II), Eu(III), Th(IV) and U(VI) aqueous complexation constants with chloro, sulphato and carbonato ligands are given in Tab. 2-7.

2.4 Estimation of uncertainties

This section describes the approach used within this report to estimate the uncertainties related to the experimental data and to the adsorption modelling. Uncertainties originate from various sources and are not always easy to quantify. In case of the application of the bottom-up approach to blind predict adsorption on natural rock samples, the most important sources of uncertainties are related to:

1. the experimental errors
2. the adsorption model and its intrinsic parameters (*i.e.*, site capacities, protolysis constants, SCCs, and selectivity coefficients)
3. the variation of the heterogeneous natural system (*i.e.*, uncertainties on the mineralogical composition, on the adsorption properties of the different clay minerals compared to the reference clay minerals used in the model development, etc.)
4. the uncertainty of the aqueous complexation constants

2.4.1 Uncertainty on the experimental data

Every experimental measurement contains a certain amount of uncertainty or error. A formal estimate of the experimental error can be obtained by considering the maximum error in each experimental operation step (Baeyens & Bradbury 1995). Over the years, a large amount of batch adsorption experiments repeatedly have been carried out within our research group on different clay batches, by different technicians, for various elements and at different experimental conditions (e.g. high/low adsorption and high/low solid ratio). By considering all these potential error sources (*i.e.*, systematic, random and personal error), an uncertainty of ± 60% on the R_d appears to be a realistic value. This value has been generally applied to all experimental data presented in this study.

2.4.2 Uncertainties on the modelling

In their present state, the GCS and 2SPNE SC/CE models do not provide intrinsic uncertainties for their parameters (*i.e.*, site capacities, protolysis and SCCs). In the past, the models were developed by fitting by eye the experimental data and consequently did not allow a rigorous uncertainty analysis of the constants and parameters obtained from the fitting procedure.

Since uncertainties related to modelling predictions are an important issue for the calculated values in a safety assessment of the deep geological repository (e.g. Ayoub et al. 2020), the uncertainty of the SCCs for the different elements investigated on illite and montmorillonite to this point are estimated by using the GEMSFITS code (Miron et al. 2015) in an on-going study. The methodology will be presented in an upcoming publication on the measured data from Nagra's deep drilling campaign, with the methodology and the re-evaluated data being applied in the development of the SDB for the safety assessment for the general license application.

2.4.2.1 Uncertainty on the adsorption site capacities

The adsorption models were developed on purified illite (reference systems), thus the clay minerals in the rock samples might not exhibit exactly the same adsorption characteristics as the reference clays. The only, extremely laborious way of clearly assessing the adsorption capacities and properties of the clay minerals in the rock samples would be to extract the pure clay fractions and develop a model on the extracted clay fraction.

Cation exchange: In the case of Cs(I), the adsorption values were derived from the GCS model. In the original publication (Bradbury & Baeyens 1998, 2000) it was clearly shown that the model predictions on pure illite could re-produce the experimental data within a factor of 2 to 3. In this study, the FES and T2S are estimated from the mineralogical compositions of the natural rocks (and not from pure illite studies) and an uncertainty factor of 2 on these two sites (*i.e.*, ± 0.3 log units) was considered for all Cs(I) isotherms.

Surface complexation: In the case of the 2SPNE SC/CE model a similar approach is followed. An uncertainty factor of 2 for the strong sites is considered realistic in the blind prediction of the experimental data. No uncertainty is assumed for the capacity of the weak and planar sites since they only play a role at high metal concentrations.

2.4.2.2 Uncertainty on the speciation

Aqueous speciation, particularly in natural environments, plays an important role for the adsorption of metals on sorbents. The 2SPNE SC/CE model was developed in simple background electrolytes ($NaCl/NaClO_4$) and only the adsorption of free cationic and hydrolysed species is considered. In natural systems the presence of inorganic ligands such as chloro, sulphato and carbonato complexes may considerably influence the adsorption. Since these complexes are assumed to be non-sorbing their formation in the porewater will reduce the adsorption. Depending on the strength of the thermodynamic complexation constant and the associated uncertainty the influence of speciation can be either relatively small or very high.

In order to illustrate the importance of aqueous complexation, an overview of the speciation of Ni(II), Co(II), Eu(III), Th(IV) and U(VI) calculated in the different porewaters considered in this report are given in Tab. 2-8. Cs(I) is not included in this table since it is generally weakly complexing and does not form aqueous complexes in the considered porewaters.

In the case of Ni(II) and Co(II), the aqueous speciation is of minor importance for two reasons: (i) max. 30% of Ni(II) form non-sorbing complexes, leading to a maximum adsorption reduction of ~ 0.1 log unit on the log R_d scale, and (ii) the uncertainty on the thermodynamic constant of the dominate aqueous $NiSO_4^o$ complex is only ± 0.03.

For Eu(III), the aqueous speciation plays a significant role in the sorption reduction. Eu(III) forms strong aqueous carbonate complexes. $EuCO_3^+$ is the dominant complex in nearly all porewaters (up to 76%) and the uncertainty of ± 0.4 associated with this complexation constant (log K value) can lead to a significant uncertainty range in the adsorption modelling. It should be noted that there is some experimental and spectroscopic evidence that $EuCO_3^+$ moderately sorbs on the clay surface (Marques Fernandes et al. 2010, 2015, 2016). In the applied conservative bottom-up approach in this report, however, only the free cation and the hydrolysed species are assumed to sorb.

For U(VI), the influence of carbonate on the aqueous speciation is extremely important. Up to 99% of U(VI) is present as non-sorbing $UO_2Ca_x(CO3)^{x-}$ complexes in nearly all porewaters considered, leading to a considerable adsorption reduction. The uncertainty on the modelling is accordingly large since both complexes have uncertainties of ± 0.25 and ± 0.5 on their log K values, respectively.

The influence of the uncertainty associated with the aqueous complexation constants on the adsorption modelling is graphically illustrated for the case of Th(IV) (Fig. 2-1) based on the speciation calculations given in Tab. 2-8. This table indicates that in the high pCO_2 porewater (pH 6.3), $Th(CO_3)_2(OH)_2^{2-}$ is the dominant aqueous species and consequently reduces the

adsorption. Considering the uncertainty of ± 0.5 on the thermodynamic constant leads to an uncertainty range of nearly ± 1 log unit for the blind prediction. In cases where the presence of this aqueous complex is minor (e.g. Boda Claystone and Mont Terri Opalinus Clay at pH 8) the contribution of the uncertainty considerably decreases. This is illustrated in Fig. 2-1a to 2.1d for the aforementioned four cases by the dotted/dashed blue curves.

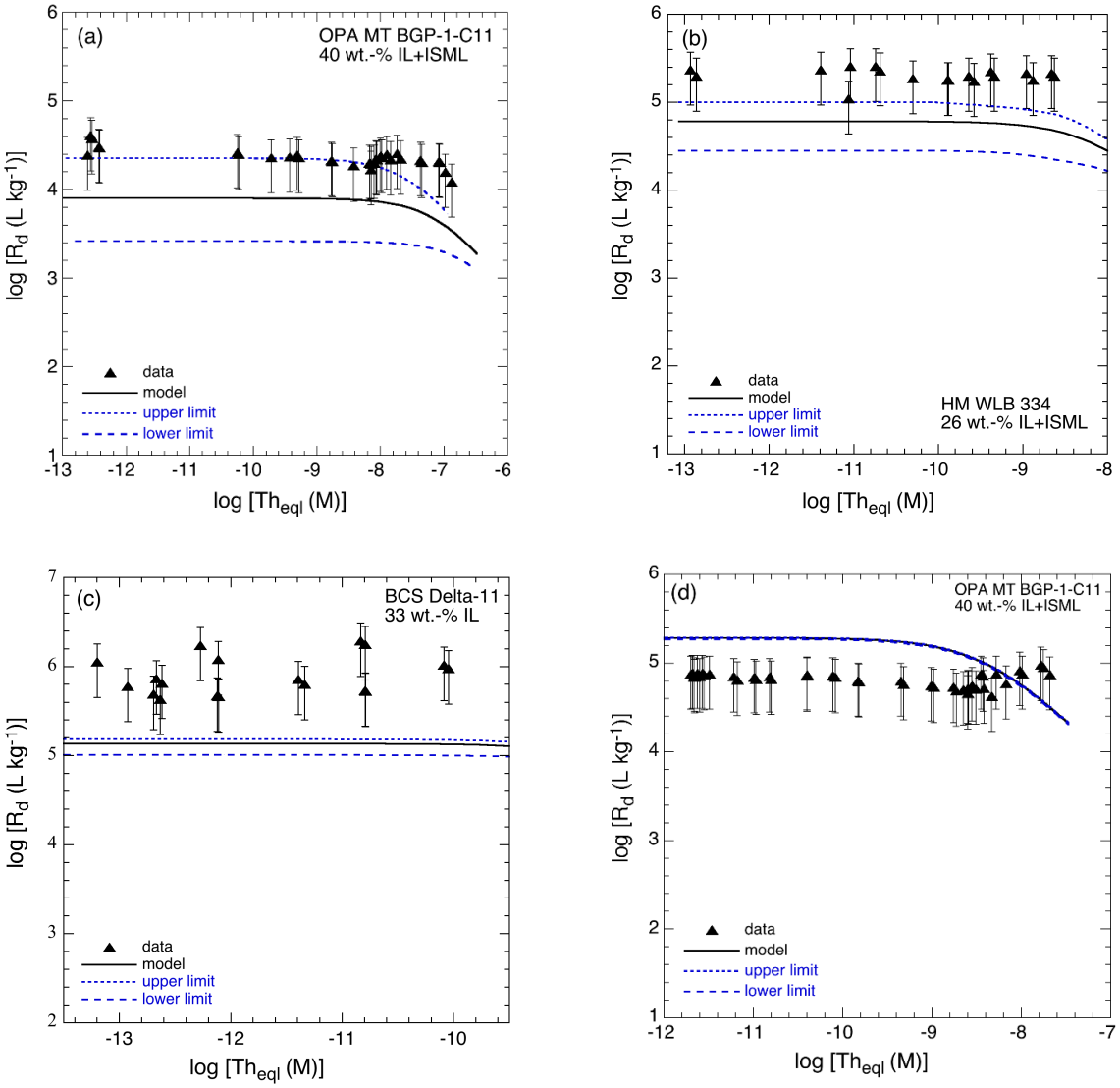

Fig. 2-1: Sorption measurements and modelling for Th(IV) on four different rock samples with varying contributions of the non sorbing $Th(CO_3)_2(OH)_2^{2-}$ in the aqueous phase, (a) 94.6%, (b) 43.5%, (c) 10.7% and (d) 1.4% (see Tab. 2-8)

The dotted/dashed blue curves illustrate the influence of speciation on the modelling arising from uncertainty in the aqueous thermodynamic constant of the $Th(CO_3)_2(OH)_2^{2-}$ complex in the aqueous phase.

Tab. 2-8 Main aqueous species for Ni(II), Eu(III), Th(IV) and U(VI) in the different porewater compositions

Formation		**Opalinus Clay**			**«Brauner Dogger»**		**Effingen Member**		**Helvetic Marl**	**Boda Claystone**
Porewater composition		Tab. 3-2		Tab. 3-6	Tab. 3-8	Tab. 3-10	Tab. 3-12	Tab. 3-14	Tab. 3-16	Tab. 3-18
pH		6.3	8.0	7.75	7.95	7.93	7.7	7.7	8.5	8.0
Main species	**log K**	**Distribution of the main species in the liquid phase** [in %]								
Ni^{2+}	-	68.0	73.2	71.3	65.9	70.7	77.3	77.7	88.1	89.0
$NiCl^{+}$	0.08 (± 0.6)	4.6	7.7	4.2	3.9	4.2	16.8	16.8	6.3	1.3
$NiHCO_3^{+}$	11.72	4.4	< 1	< 1	< 1	< 1	< 1	< 1	< 1	< 1
$NiCO_3^{o}$								< 1	4.6	
$NiSO_4^{0}$	2.35 (± 0.03)	22.9	18.5	23.4	28.8	24.2	5.3	5.2	< 1	7.5
Co^{2+}	-	-	63.3	66.3	61.9	65.9	55.3	55.8	-	86.6
$CoCl^{+}$	0.57 (± 0.6)	-	20.6	12.2	11.3	12.1	37.1	37.3	-	3.7
$CoSO_4^{0}$	2.30 (± 0.03)	-	14.2	19.3	24.1	20.1	3.4	3.4	-	6.5
Eu^{3+} + $EuOH^{2+}$ + $Eu(OH)_2^{+}$	-	13.0	38.5	14.7	13.5	14.3	46.9	46.8	6.1	9.9
$EuCO_3^{+}$	8.0 (± 0.4)	70.7	50.2	70.5	68.7	69.5	43.6	43.6	49.5	76.0
$Eu(CO_3)_2^{-}$	12.9 (± 0.6)	3.4	1.9	5.1	6.7	6.3	0.6	0.6	43.8	13.6
$EuSO_4^{+}$	3.3 (± 0.15)	11.7	8.3	7.3	7.1	6.0	4.6	4.6	-	< 1
$Th(OH)_3^{+}$ + $Th(OH)_4^{0}$	-	4.9	98.6	86.2	89.6	90.1	99.3	99.3	56.2	89.3
$Th(CO_3)_2(OH)_2^{2-}$	8.8 (± 0.5)	94.6	1.4	13.7	10.5	9.9	0.7	0.7	43.5	10.7
$UO_2(OH)_2^{0}$ + $UO_2(OH)_3^{-}$	-	< 1	< 1	< 1	< 1	< 1	< 1	< 1	< 1	< 1
$UO_2(CO_3)_3^{4-}$	21.84 (± 0.04)	-	2.0	4.4	4.8	4.4	0.4	0.5	29.6	1.9
$UO_2Mg(CO_3)_3^{2-}$	26.11 (± 0.5)	-	4.7	4.8	5.0	4.9	4.8	3.8	3.8	5.5
$UO_2Ca(CO_3)_3^{2-}$	27.18 (± 0.5)	-	75.5	81.8	82.0	81.9	57.8	57.8	60.7	84.8
$UO_2Ca_2(CO_3)_3^{0}$	29.22 (± 0.25)	-	16.4	8.0	7.5	8.1	36.6	36.6		7.0

3 Rock formations: mineralogy and porewater compositions

The present report gives an overview of the modelling of experimental sorption data obtained on different Swiss and non-Swiss sedimentary rocks (clay-rich and clay-poor (< 10 wt.-% clay mineral content) samples). The experimental data originate from different sources (Baeyens 1982, Baeyens et al. 2014, Bradbury & Baeyens 2000, De Preter et al. 1991, Marques Fernandes et al. 2015, McKinley & West 1982, Melkior et al. 2005, Savoye et al. 2012). The data obtained for Ni(II), Co(II), Eu(III) and Th(IV) on the Boda Claystone sample delta-11 are unpublished PSI data and the experimental details are given in Appendix A. This chapter summarises the mineralogy of the different samples on which sorption isotherms were measured and the associated porewater compositions.

3.1 Swiss sedimentary rocks

The following sections give a detailed overview of the mineralogical compositions of the investigated Swiss sedimentary rock samples and the compositions of the corresponding porewaters used to measure the sorption isotherms.

3.1.1 Opalinus Clay

3.1.1.1 Mont Terri rock laboratory

Tab. 3-1: Mineralogical composition of Mont Terri Opalinus Clay samples BGP-1-C11 (Lauber et al. 2000) and DI-A0-3.4 (Baeyens et al. 2014)

Mineral	**Sample BGP-1-C11** [wt.-%]	**DI-A0-3.4** [wt.-%]
Calcite	9 ± 2	13 ± 8
Dolomite/ankerite	2 ± 0.5	n.d.
Siderite	4 ± 1	3 ± 1.8
Quartz	12 ± 2	14 ± 4
K-feldspar	1.5 – 3	1 ± 1.6
Albite	1.3 ± 0.7	1 ± 1
Pyrite	n.d.	1.1 ± 0.5
C (organic)	≤ 0.4	0.8
Illite	22 ± 4	23 ± 2
Illite smectite mixed layer	18 ± 4	11 ± 2
Chlorite	10 ± 2	10 ± 2
Kaolinite	20 ± 3	22 ± 2

n.d.: not detected

Tab. 3-2: Composition of the porewater equilibrated with Opalinus Clay sample BGP-1-C11 at pH = 6.3 and pH 8 (Lauber et al. 2000) and Opalinus Clay sample DI-A0-3.4 at pH = 7.6

Pearson (1998); n.m.: not measured

	BGP-1-C11		**BGP-1-C11/DI-A0-3.4**
pH	6.3	8.0	7.6
pCO_2 [bar]	0.5*	$< 10^{-5}$	$10^{-3.5}$
I [M]	0.3	0.39	0.39
Element	**Concentration** [M]		
Na	1.87×10^{-1}	2.49×10^{-1}	2.4×10^{-1}
K	4.02×10^{-3}	5.80×10^{-3}	1.6×10^{-3}
Mg	1.42×10^{-2}	2.15×10^{-2}	1.7×10^{-2}
Ca	1.84×10^{-2}	2.88×10^{-2}	2.6×10^{-2}
Sr	2.16×10^{-4}	2.67×10^{-4}	5.1×10^{-4}
Fe	2.47×10^{-5}	4.74×10^{-6}	n.m.
Si	3.96×10^{-4}	3.01×10^{-4}	n.m.
Al	2.93×10^{-6}	5.21×10^{-6}	n.m.
Cl	1.86×10^{-1}	3.0×10^{-1}	3.0×10^{-1}
SO_4	2.92×10^{-2}	2.82×10^{-2}	1.4×10^{-2}
C_{inorg}	1.73×10^{-2}	1.78×10^{-4}	4.8×10^{-4}

* Fixed through CO_2 overpressure in the glove box

3.1.1.2 Benken

Tab. 3-3: Mineralogy of the Benken Opalinus Clay sample (636.57 – 636.67 m) used in this study

Baeyens et al. (2014)

Mineral	**Composition** [wt.-%]
Calcite	13
Dolomite/Ankerite	1
Siderite	n.d.
Quartz	15
K-Feldspar	1
Albite/Plagioclase	1
Pyrite	1.7
Illite	17
Illite smectite mixed layer	10
Kaolinite	27
Chlorite	13
Organic Carbon	0.4

n.d.: not detected

Tab. 3-4: Composition of the synthetic porewater for the Benken Opalinus Clay sample (636.57 – 636.67 m)

Pearson (2000)

pH	7.9
pCO_2 [bar]	$10^{-3.5}$
I [M]	0.20
Element	**Concentration** [M]
Na	1.60×10^{-1}
K	4.20×10^{-3}
Mg	5.18×10^{-3}
Ca	6.85×10^{-3}
Sr	3.9×10^{-4}
SO_4	1.07×10^{-2}
Cl	1.60×10^{-1}
$C_{inorg.}$	3.1×10^{-4}
Mn	3×10^{-8}
Si	2.9×10^{-5}
Al	$< 2 \times 10^{-6}$

3.1.1.3 Schlattingen-1

Tab. 3-5: Mineralogical composition of Opalinus Clay sample SLA-938 from the Schlattingen-1 borehole
Baeyens et al. (2014)

Mineral	**Composition** [wt.-%]
Calcite	7
Dolomite/Ankerite	2
Siderite	6
Quartz	9
K-Feldspar	1
Albite/Plagioclase	n.d.
Pyrite	0.9
Illite	17
Illite smectite mixed layer	30
Kaolinite	21
Chlorite	6

n.d.: not detected

Tab. 3-6: Composition of the synthetic Opalinus Clay porewater equilibrated with sample SLA-938

Wersin et al. (2013)

pH	7.5 – 7.75
pCO_2 [bar]	$10^{-3.5}$
I [M]	0.23
	Concentration (M)
Na	1.67×10^{-1}
K	3.15×10^{-3}
Mg	8.69×10^{-3}
Ca	1.21×10^{-2}
Sr	1.75×10^{-6}
SO_4	2.42×10^{-2}
Al	2.1×10^{-4}
Si	7.1×10^{-5}
Mn	8.5×10^{-7}
Fe	$< 1.8 \times 10^{-6}$
Cl	1.60×10^{-1}
$C_{inorg.}$	5.43×10^{-4}

3.1.2 «Brauner Dogger»

3.1.2.1 «Brauner Dogger» clay-rich sequences

Tab. 3-7: Mineralogical composition of «Brauner Dogger» clay-rich sequences samples from Benken, BEN-482 (Baeyens et al. 2014) and BEN-525 (Martin Mazurek, University of Bern, pers. comm.)

Mineral	**BEN-482**	**BEN-525**
	Composition [wt.-%]	
Calcite	25	12.4
Dolomite/Ankerite	2	0.5
Siderite	n.d.	n.d.
Quartz	21	54.9
K-Feldspar	2	11.5
Albite/Plagioclase	1	n.d.
Pyrite	1.5	0.8
Illite	11	8.5
Illite smectite mixed layer	15	7.7
Kaolinite	17	2
Chlorite	4	1.6

n.d.: not detected

Tab. 3-8: Composition of the porewater equilibrated with «Brauner Dogger» clay-rich sequences samples from Benken BEN-482 and BEN-525

Baeyens et al. (2014)

pH	7.9 – 8.1	
pCO_2 [bar]	$10^{-3.5}$	
I [M]	0.23	
Element	**BEN-482**	**BEN-525**
	Concentration [M]	
Na	1.65×10^{-1}	1.70×10^{-1}
K	2.77×10^{-3}	3.16×10^{-3}
Mg	9.15×10^{-3}	8.91×10^{-3}
Ca	1.23×10^{-2}	2.07×10^{-2}
Sr	1.34×10^{-6}	1.47×10^{-6}
SO_4	3.21×10^{-2}	2.49×10^{-2}
Al	6.2×10^{-6}	2.4×10^{-4}
Si	5.3×10^{-5}	4.3×10^{-5}
Mn	7.6×10^{-7}	1.5×10^{-6}
Fe	$< 1.8 \times 10^{-6}$	$< 1.8 \times 10^{-7}$
Cl	1.60×10^{-1}	1.60×10^{-1}
C_{inorg}	5.43×10^{-4}	5.43×10^{-4}

3.1.2.2 «Brauner Dogger» sandy limestone sequences

Tab. 3-9: Mineralogical composition of «Brauner Dogger» sandy limestone sequences sample SLA-795 from Schlattingen-1

Baeyens et al. (2014)

Mineral	**Composition** [wt.-%]
Calcite	85
Dolomite/Ankerite	2
Siderite	1
Quartz	7
K-Feldspar	1
Albite	n.d.
Pyrite	0.2
Illite	0.8
Illite smectite mixed layer	2.7
Kaolinite	0.3
Chlorite	0.4

n.d.: not detected

Tab. 3-10: Composition of the porewater equilibrated with «Brauner Dogger» sandy limestone sequences sample SLA-795

Baeyens et al. (2014)

pH	7.9 – 8.0
pCO_2 (bar)	$10^{-3.5}$
I (M)	0.39
Element	**Concentration (M)**
Na	1.69×10^{-1}
K	3.45×10^{-3}
Mg	8.94×10^{-3}
Ca	1.24×10^{-2}
Sr	8.50×10^{-7}
SO_4	2.55×10^{-2}
Al	4.1×10^{-5}
Si	$< 3.6 \times 10^{-5}$
Mn	$< 5.0 \times 10^{-7}$
Fe	$< 2.0 \times 10^{-6}$
Cl	1.60×10^{-1}
$C_{inorg.}$	5.43×10^{-4}

3.1.3 Effingen Member

3.1.3.1 Effingen Member calcareous marl sequences

Tab. 3-11: Mineralogy of Effingen Member calcareous marl sequences sample OFT-619
Baeyens et al. (2014)

Mineral	**Composition** [wt.-%]
Calcite	43
Dolomite/Ankerite	3
Siderite	n.d.
Quartz	14
K-Feldspar	1
Albite/Plagioclase	0
Pyrite	0.7
Illite	10
Illite smectite mixed layer	9
Kaolinite	12
Chlorite	6

n.d.: not detected

Tab. 3-12: Porewater composition of Effingen Member sample OFT-619
Baeyens et al. (2014)

pH	7.5 – 7.8
pCO_2 [bar]	$10^{-3.5}$
I [M]	0.7 M
Element	**Concentration** [M]
Na	3.72×10^{-1}
K	2.00×10^{-3}
Mg	4.38×10^{-2}
Ca	6.35×10^{-2}
Sr	9.25×10^{-4}
SO_4	1.17×10^{-2}
Al	$< 3.7 \times 10^{-6}$
Si	3.41×10^{-5}
Cl	5.66×10^{-1}
$C_{inorg.}$	1.73×10^{-4}

3.1.3.2 Effingen Member limestone sequences

Tab. 3-13: Mineralogical composition of Effingen Member Limestone sequences sample OFT-492

Baeyens et al. (2014)

Mineral	**Composition** [wt.-%]
Calcite	77
Dolomite/Ankerite	3
Siderite	n.d.
Quartz	7
K-Feldspar	< 1
Albite/Plagioclase	< 1
Pyrite	1.0
Illite	3
Illite smectite mixed layer	4
Kaolinite	4
Chlorite	< 1

n.d.: not detected

Tab. 3-14: Composition of the porewater equilibrated with the Effingen Member limestone sequences sample OFT-492

Baeyens et al. (2014)

pH	7.7
pCO_2 [bar]	$10^{-3.5}$
I [M]	0.7
Element	**Concentration** [M]
Na	3.74×10^{-1}
K	2.49×10^{-3}
Mg	4.69×10^{-2}
Ca	6.02×10^{-2}
Sr	7.94×10^{-4}
SO_4	1.14×10^{-2}
Al	3.30×10^{-5}
Si	1.49×10^{-4}
Cl	5.66×10^{-1}
$C_{inorg.}$	1.73×10^{-4}

3.1.4 Helvetic Marl

Tab. 3-15: Mineralogical composition of the Helvetic Marl sample WLB-334
Baeyens et al. (2014)

Mineral	**Composition** [wt.-%]
Calcite	51
Dolomite/Ankerite	4
Quartz	11
K-Feldspar	1
Pyrite	1.1
Illite	13
Illite smectite mixed layer	13
Kaolinite	0
Chlorite	6

Tab. 3-16: Composition of porewaters equilibrated with the Helvetic Marl sample WLB-334 Baeyens et al. (2014)

pH	8.3 – 8.6
pCO_2 [bar]	$10^{-3.5}$
I [M]	0.206
Element	**Concentration** [M]
Na	1.98×10^{-1}
K	2.3×10^{-3}
Mg	7.8×10^{-4}
Ca	1.1×10^{-3}
Sr	1.9×10^{-4}
SO_4	2.1×10^{-4}
Si	4.6×10^{-5}
Al	1.1×10^{-5}
Cl	2.02×10^{-1}
$C_{inorg.}$	1.54×10^{-3}

3.2 Non-Swiss argillaceous rocks

The mineralogical composition of the non-Swiss argillaceous samples investigated (*i.e.*, Boom Clay from Belgium (BC), Callovo-Oxfordian Clay (COx) from France, Oxford Clay (OxC) from the United Kingdom and Boda Claystone (BCS) from Hungary), and the composition of the porewaters associated with these samples, are provided in the Tabs. 3-17 and 3-18.

Tab. 3-17: Mineralogical composition of COx (Savoye et al. 2012), BC (Griffault et al. 1996), OxC (McKinley & West 1982) and BCS (Breitner et al. 2015, Marques Fernandes et al. 2015)

Mineral composition [wt.-%]	**COx**	**BC**	**OxC**	**BCS**	
				Ib-4	**delta-11**
Quartz	18 – 26	20	9 – 30	8	1.8
K-Feldspar		5 – 10	Trace	17	5
Na-plagioclase	-	-	-	-	36.6
Carbonates	20 – 31	1 – 5	2 – 40	8	13
Siderite		-	-	-	-
Pyrite		1 – 5	1 – 5	-	-
Hematite				6	7.2
Analcime				10	0.6
Accessory minerals	< 5				-
Illite	8.3 – 16.9	25 ± 5	26 ± 10	50	33
Illite smectite mixed layer	20.8 – 42.3	5 – 10	-	-	-
Smectite	2.9 – 5.9	10 – 20	4 – 48	-	-
Chlorite	0.3 – 0.7	5 – 20	Trace to 18	-	3.2
Kaolinite	0.6 – 1.3	20 – 30	Trace to 20	-	-
Chlorite smectite mixed layer	-	5 – 10	-	-	-

Tab. 3-18: Synthetic porewater compositions of COx (Melkior et al. 2005, Savoye et al. 2012), BC, OxC and BCS

	COx		**BC**	**OxC**	**BCS (Ib-4 and delta-11)**
pH	7.8	7.0	8.8	7 – 7.5	8.0
I [M]	0.06	0.09	0.025	0.19	0.033
Element	**Concentration** [M]				
Na	7.3×10^{-3}	5.2×10^{-2}	2.9×10^{-2}	1.6×10^{-1}	1.7×10^{-2}
K	2.5×10^{-3}	1.0×10^{-3}	1.0×10^{-3}	1.1×10^{-5}	1.8×10^{-4}
NH_4	-	-	-	2.4×10^{-4}	-
Ca	8.1×10^{-3}	6.4×10^{-3}	-	6.0×10^{-3}	3.1×10^{-3}
Mg	6.5×10^{-3}	4.5×10^{-3}	5.0×10^{-4}	-	2.4×10^{-3}
Sr	-	-	-	1.2×10^{-4}	-
Cl	4.1×10^{-2}	4.1×10^{-2}	2.0×10^{-3}	1.7×10^{-1}	2.3×10^{-2}
$C_{inorg.}$	3.7×10^{-4}	1.6×10^{-2}	1.5×10^{-2}	1.0×10^{-4}	6.1×10^{-4}
S/SO_4	3.5×10^{-2}	2.6×10^{-3}	-	4.6×10^{-3}	1.9×10^{-3}
F	-	-	1.5×10^{-3}	4.2×10^{-5}	-

4 Caesium

This chapter compiles 16 caesium isotherms (12 in-house and 4 data sets taken from the open literature) measured on different sedimentary rocks in their corresponding porewater. Each individual isotherm is modelled with the GCS model (Bradbury & Baeyens 2000) as described in Section 2.1. As discussed before the uncertainty of the GCS model is assumed to arise essentially from the uncertainty associated with the FES and T2S capacities and is assumed to be a factor of 2 (reflected by the upper and lower limit curves in the figures). The estimated uncertainty of the experimental data estimated at ± 60% is illustrated by the error bars.

The deviation between the model calculations (blind predictions) and the experimental data points indicates whether the bottom-up approach is an appropriate methodology to predict adsorption on different types of sedimentary rocks. If the error bars of the experimental data lie within the uncertainty range of the modelling, the prediction from bottom-up approach can be considered as reliable.

The adsorption values for Cs(I) were predicted with the GCS model by scaling the site capacities (Q) of the FES and T2S to the illite content of the considered rock sample in its porewater composition, with:

$$Q_{FES} = F_{illite} \times CEC_{illite} \times 0.0025$$
$$Q_{T2S} = F_{illite} \times CEC_{illite} \times 0.2$$

where F_{illite} = wt.-% illite/100, CEC_{illite} = 200 meq kg^{-1}, and 0.0025 and 0.2 are the fractions of FES and T2S, respectively. The CEC of the PS corresponds to the measured CEC of the rock minus the contribution of the T2S. The site capacities of the three different sites are non-adjustable parameters in the modelling procedure. The competitive exchange with Na, K, Mg and Ca on the PS, and Na, K (and NH_4) on FES and T2S, are controlled by the reactions and selectivity coefficients given in Tab. 2-2.

4.1 Cs(I) isotherms on Opalinus Clay

4.1.1 Mont Terri rock laboratory

The Cs(I) sorption isotherms presented in Fig. 4-1 were carried out by Lauber et al. (2000) in the framework of Project Opalinus Clay (Nagra 2002). The illite contents and porewater compositions are given in Tabs. 3-1 and 3.2, respectively. The model calculations describe the isotherms very well (in terms of shape and R_d value). The R_d values on the FES for the isotherm at pH 6.3 are slightly underpredicted but still fall within the error range of the experimental data.

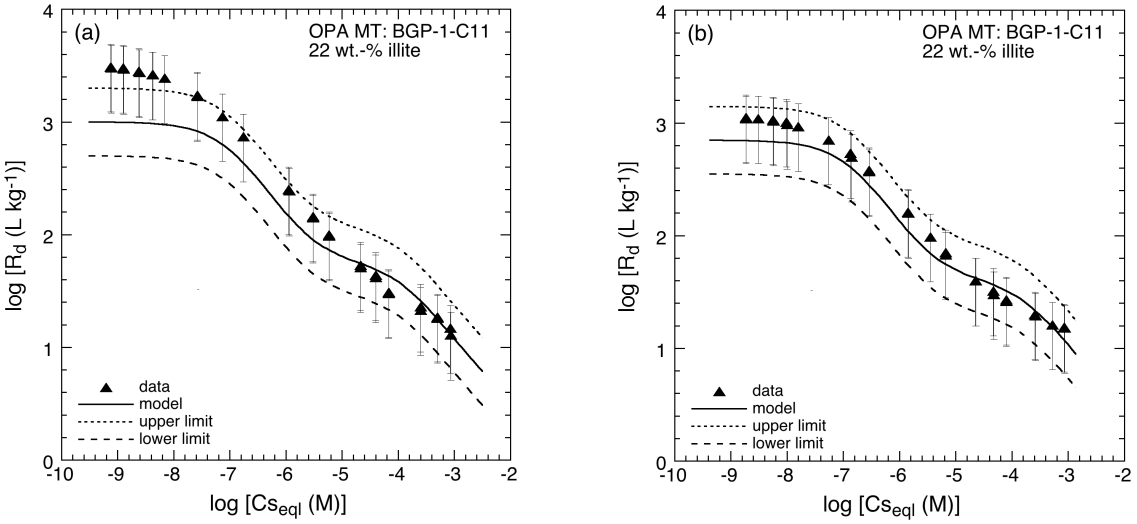

Fig. 4-1: Sorption measurements and modelling for Cs(I) on Mont Terri Opalinus Clay sample BGP-1-C11 at (a) pH 6.3 and (b) pH 8 in the synthetic pore water given in Tab. 3-2

Data from Lauber et al. (2000)

The data given in Fig. 4-2 originate from a study by Van Loon et al. (2009), in which the transferability of the Cs(I) sorption measurements from dispersed to compacted systems was studied. The Opalinus Clay sample originated from the DI field experiment at the Mont Terri rock laboratory. The blind prediction overestimates sorption by ~ 0.4 log units at $[Cs_{eql}] > 10^{-5}$ M, but the lower limit of the model is still within the upper limit error bars of the measurements.

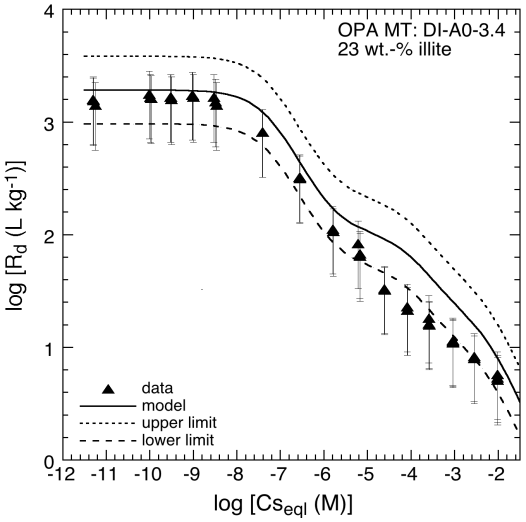

Fig. 4-2: Sorption measurements and modelling for Cs(I) on Opalinus Clay sample DI-A0-3.4 from the DI field experiment in the Mont Terri rock laboratory

Data from Van Loon et al. (2009)

4.1.2 Opalinus Clay from Benken and Schlattingen-1

Deep drilling campaigns carried out in Benken (Canton Zürich) and Schlattingen (Canton Thurgau) provided samples on which Cs(I) sorption isotherms were determined. Fig. 4-3 shows the experimental results on these samples. With the illite contents given in Tabs. 3-3 and 3-5, and the porewater compositions given in Tabs. 3-4 and 3-6, blind predictions were made and are illustrated by the solid lines in Fig. 4-3. The prediction for the Benken sample is very good and is within the error bars of the measurements. The data for the Schlattingen-1 sample are underpredicted over the entire Cs concentration range but are still within the upper limit of the modelled uncertainty range.

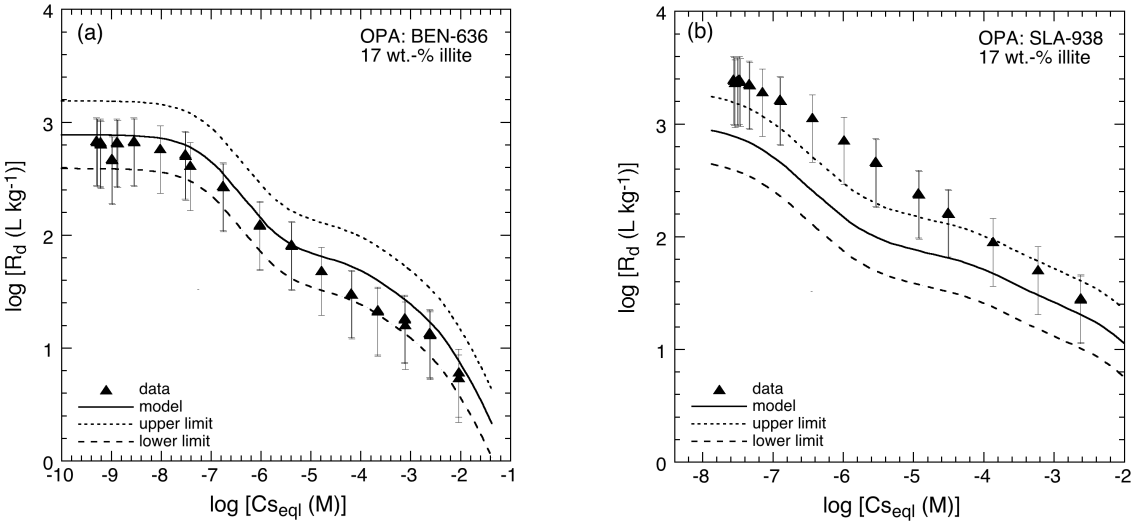

Fig. 4-3: Sorption measurements and modelling for Cs(I) on Opalinus Clay samples from (a) Benken (BEN-636) and (b) Schlattingen-1 (SLA-938)

Data from Baeyens et al. (2014)

4.2 Cs(I) isotherms on «Brauner Dogger» and Effingen Member samples

The geological formation «Brauner Dogger» and the Effingen Member are situated stratigraphically above the Opalinus Clay. They have similar mineralogical compositions compared to Opalinus Clay but have a much lower 2:1 clay mineral content. In the sandy limestone sequences of «Brauner Dogger» the illite content is only 0.8 wt.-%. The illite content and porewater compositions are given in Tabs. 3-7 to 3-14.

The results of the Cs(I) sorption isotherms on the «Brauner Dogger» samples are shown in Fig. 4-4. The samples exhibiting an illite content of ~ 10 wt.-% are reasonably well described by the model calculations and are generally within the error bars of the measurements except for the [Cs_{eql}] range between 10^{-7} and 10^{-5} M (range where T2S dominate), where the deviations reach maximal ~ 0.4 to 0.7 log units.

The blind prediction of the Cs(I) adsorption on the clay-poor sample SLA-795 (Fig. 4-4c) underpredicts the experimental data over the entire [Cs_{eql}] range (by max. 0.8 log units). It should be noted that the illite content is very low in this sample (0.8 wt.-%) and contributions from the ISML are also not considered.

Nonetheless, the trend in the experimental data is fully in agreement with the decreasing illite content; sorption values at ~ 10 wt.-% illite are almost one order of magnitude higher compared to the «Brauner Dogger» sample exhibiting only ~ 1 wt.-% illite.

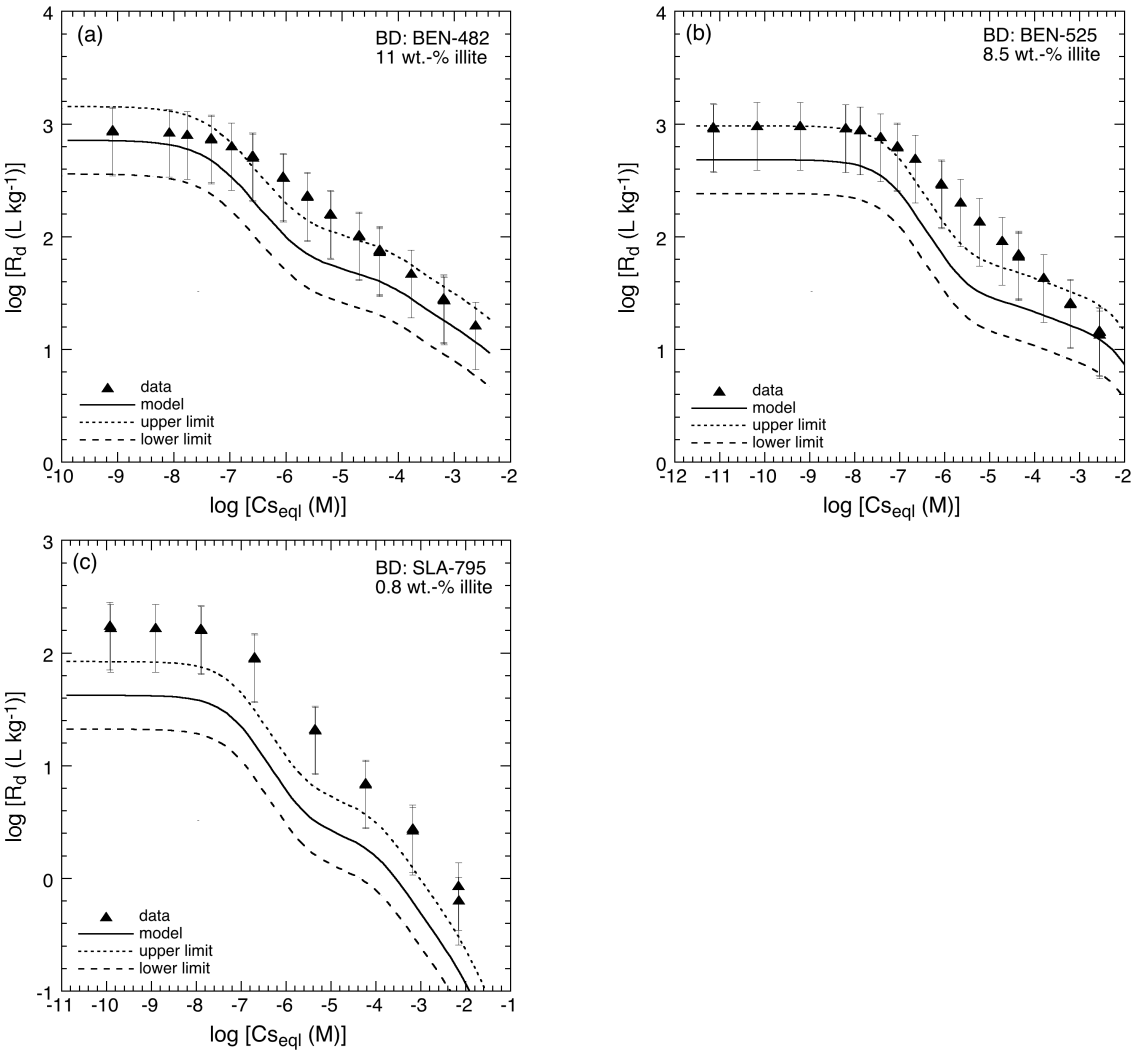

Fig. 4-4: Sorption measurements and modelling for Cs(I) on «Brauner Dogger» clay-rich sequences samples (a) BEN-482 and (b) BEN-525, and for «Brauner Dogger» sandy-limestone sequences sample (c) SLA-795

Data from Baeyens et al. (2014)

The results of the Cs isotherms on the Effingen Member samples are shown in Fig. 4-5. The prediction of the Cs isotherm on the OFT-619 sample is very good and lies within the error bars of the measurements over the entire [Cs_{eql}] range.

The Cs isotherm on the comparatively clay-poor OFT-492 sample is underpredicted by 0.4 to 0.7 log units over the whole [Cs_{eql}] range. Similar to the Cs isotherms on the «Brauner Dogger» samples (Fig. 4-4), the blind prediction of this sample fails to re-produce the shape of the isotherms in the middle [Cs_{eql}] range, where T2S are supposed to be the dominating sites. Nonetheless, error ranges of the measurements correlate with the uncertainty range of the blind prediction.

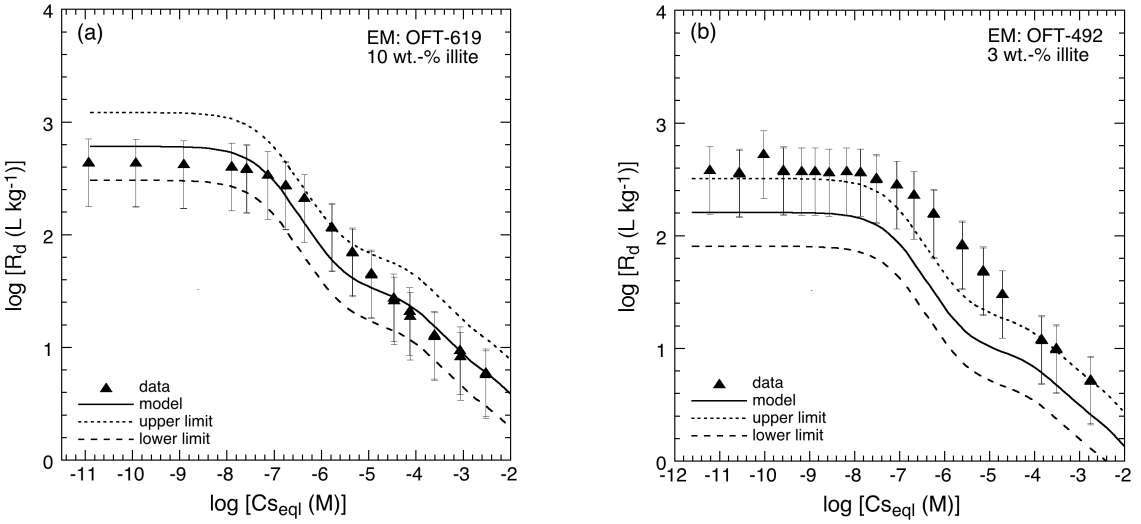

Fig. 4-5: Sorption measurements and modelling for Cs(I) on Effingen Member (a) calcareous marl sample OFT-619and (b) limestone sequences sample OFT-492

Data from Baeyens et al. (2014)

4.3 Cs(I) isotherm on Helvetic Marl

Cs(I) isotherms have been measured on Helvetic Marl sample WLB-334 (Baeyens et al. 2014) and the results are shown in Fig. 4-6 together with modelling. Marl formations are strongly dominated by carbonates (see Tab. 3-15), however, exhibit up to 13 – 14 wt.-% illite. The composition of the synthetic porewater is given in Tab. 3-16.

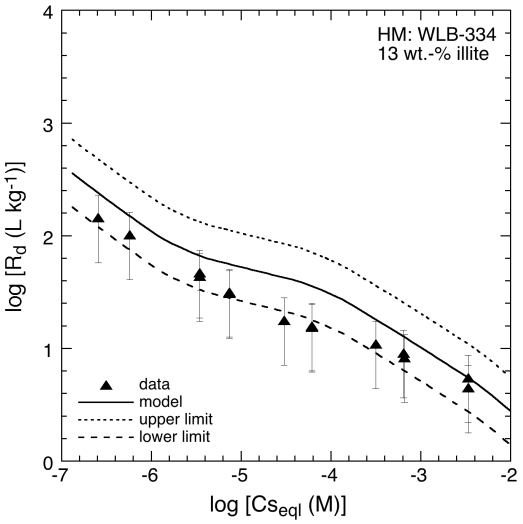

Fig. 4-6: Sorption measurements and modelling for Cs(I) on Helvetic Marl sample WLB-334

Data from Baeyens et al. (2014)

The predictions of the Cs isotherm measured on the marl sample are at the lower limit of the model calculations, while both exhibit a very similar shape.

4.4 Cs(I) isotherms on non-Swiss argillaceous rocks

Argillaceous rocks are considered in different countries as potential host rocks for the disposal of radioactive waste. Cs(I) isotherms available in the open literature have been considered in this study, including data from BC, Cox, OxC and BCS. The mineralogical compositions of the rock samples on which the Cs(I) isotherms have been determined are summarised in Tab. 3-17. The synthetic porewater compositions are summarised in Tab. 3-18. The data from BC originate from Baeyens (1982) and De Preter et al. (1991). Cs(I) isotherms on COx were taken from Melkior et al. (2005) and Savoye et al. (2012). The sorption data for COx are taken from McKinley & West (1982). Note that in the latter study the porewater contained substantial amounts of NH_4, which is similar to K, an important competitive cation for the sorption of Cs(I) on illite. For this reason, the selectivity coefficients derived by Wick et al. (2018) for the ion equilibria of NH_4^+ towards Na^+ on the three sorption sites have been included in the calculations and the K_c values used in the modelling are included in Tab. 2-2. BCS data are taken from Marques Fernandes et al. (2015). The experimental data and modelling for these four types of argillaceous rocks are summarised in Fig. 4-7.

The prediction of the Cs(I) isotherms measured on the non-Swiss argillaceous rocks are very good. With exception of BCS, where the sorption on T2S is slightly overpredicted, the calculations on FES and T2S are within the experimental error bars. Note that FES were not necessary to model the Cs(I) isotherm on BCS. The underprediction of the Cs(I) sorption on the PS for COx (Fig. 4-7b) and for OxC (Fig. 4-7d) at very high [Cs_{eql}] (0.01 M to 0.1 M) are likely due to the contribution of Cs(I) sorption on the planar sites of smectite and ISML (see Tab. 3-17), which are not considered in the modelling.

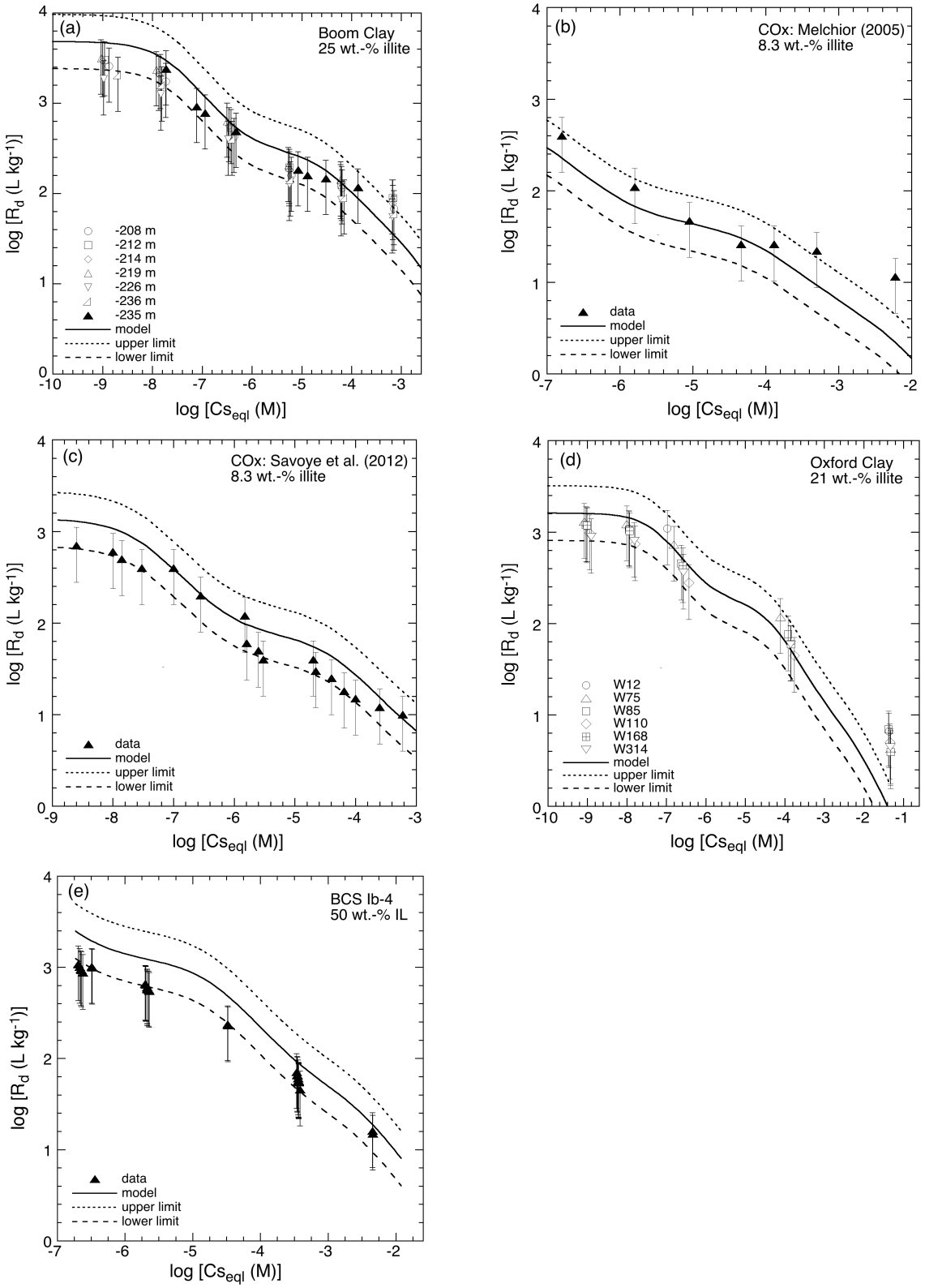

Fig. 4-7: Sorption measurements and modelling for Cs(I) on (a) BC (data from Baeyens 1982, and De Preter et al. 1991), (b, c) COx (data from Melchior et al. 2005 and Savoye et al. 2012), (d) OxC (data from McKinley & West 1982) and (e) BCS (data from Marques Fernandes et al. 2015)

4.5 Summary

Sixteen different Cs(I) isotherms have been compiled and modelled with the GCS model (Bradbury & Baeyens 2000). All model calculations were performed with the non-adjusted site capacities (which are directly related to the illite content of each rock sample) and the selectivity coefficients as given in Tab. 2-5. Uncertainty limits have been calculated considering that the site capacities of the FES and T2S can vary by a factor of 2 for the default values tabulated in Tab. 2-2.

All Cs(I) isotherms measured on the different rock formation exhibit the typical non–linear uptake behaviour of Cs on different site types in agreement with sorption dominated by illite. The Cs sorption measurements and the blind predictions show a good to very good agreement considering that the experimental data were obtained by different laboratories on different types of rocks with different illite contents (ranging from ~ 1 wt.-% to 30 wt.-%) and in different porewater compositions. In view of the applied uncertainties on the experimental data and modelling, all isotherms can be quantitatively described by the GCS model. Only few experimental data points clearly fall outside the uncertainty ranges applied to the data and modelling.

5 Nickel and Cobalt

This chapter presents sorption measurements and modelling of Ni(II) and Co(II) isotherms on the different rocks using the corresponding 2SPNE SC/CE adsorption model for illite scaled to the 2:1 clay mineral content and by taking into account the aqueous speciation in the given porewater (see Section 2.2). Both transition metals adsorb essentially by surface complexation in the investigated pH range, contributions from cation exchange on the planar sites are negligible. The model, the associated parameters and SCCs as well as the aqueous thermodynamic data are summarised in Chapter 2. The mineralogical compositions of the rock samples and porewater compositions are summarised in Chapter 3. The adsorption behaviour of Ni(II) and Co(II) on clay minerals, both divalent transition metals, is very similar and therefore the data are presented together in this chapter. The uncertainty on the modelling was estimated, as described in Section 2.4, from the uncertainty on the capacity of strong sites, which control adsorption in the trace concentration range and the uncertainty on the aqueous speciation. The influence of competing cations on the sorption of Ni(II) and Co(II) on the strong sites was not considered (Marques Fernandes & Baeyens 2020). Blind predicted data are illustrated by the solid black line, dashed lines represent the uncertainty range of the modelling in the figures in this chapter.

5.1 Ni(II) and Co(II) isotherms on Opalinus Clay

5.1.1 Opalinus Clay from Mont Terri rock laboratory

Two Ni(II) and two Co(II) sorption isotherms were measured on Opalinus Clay samples from the Mont Terri rock laboratory. The mineralogical and porewater compositions are given in Tabs. 3-1 and 3-2, respectively.

Nickel

Fig. 5-1 shows the Ni(II) sorption isotherms on Mont Terri Opalinus Clay sample BGP-1-C11 measured in two different porewaters (Lauber et al. 2000; see Tab. 3-2). The blind prediction at pH 6.3 (Fig. 5-1a) overestimates the experimental data whereas the isotherm measured at pH 7.8 (Fig. 5-1b) is underestimated by the predictive calculation. The deviations are within ± 0.5 log units except for the isotherm at pH 8 where the discrepancies are higher. The sharply increasing sorption values at low Ni_{eql} concentrations are not understood. With increasing [Ni_{eql}] (10^{-5} M) the sorption values steadily deviate (by increasing) from the modelled curves. Increasing the value of the SCC of the first Ni complex on the weak sites ($\equiv S^{W}ONi^{+}$) does not allow re-producing the shape of the experimental data. The precipitation of a solubility controlling Ni(II) phase such as Ni-(hydr)oxide or Ni-carbonate can be excluded since this would probably lead to a sharp increase of the uptake around the solubility limiting Ni(II) concentration, suggesting that another mechanism might control the uptake in this concentration range (see Section 5.6).

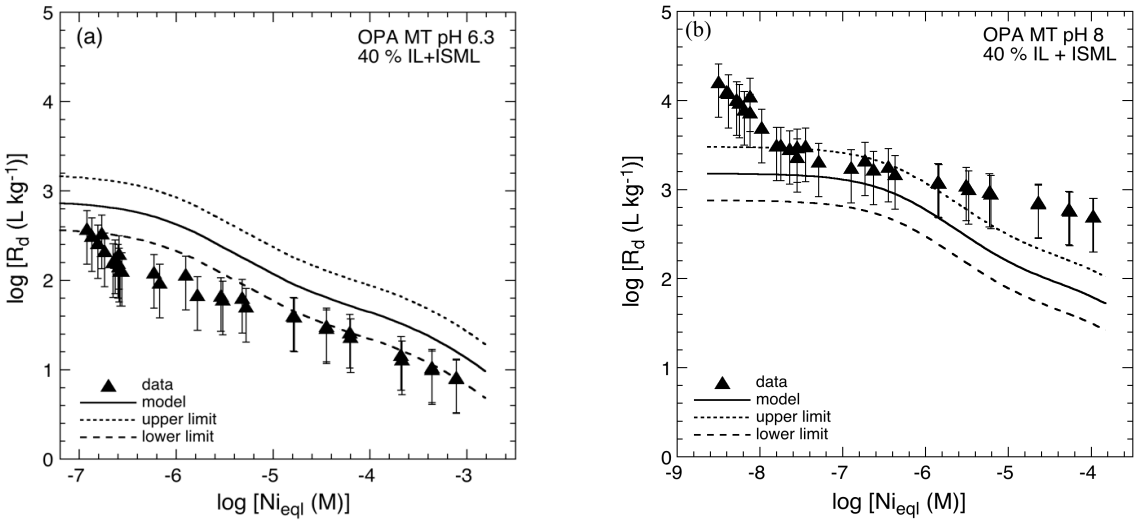

Fig. 5-1: Sorption measurements and modelling for Ni(II) on Mont Terri Opalinus Clay sample BGP-1-C11 at (a) pH 6.3 and (b) pH 7.8

Data taken from Lauber et al. (2000)

Cobalt

Fig. 5-2 shows two Co(II) isotherms on Opalinus Clay sample DI-A0-3.2 originating from the DI experiment at Mont Terri (Baeyens et al. 2014) and Mont Terri sample BGP-1-C11 (Bradbury & Baeyens 2011) measured in the same porewater (Pearson 1998). The blind prediction of the Co(II) adsorption on DI-A0-3.2 (Fig. 5-2a) overestimates the experimental data at low [Co_{eql}] by around one order of magnitude. For this part of the isotherm, one can consider that the bottom-up approach as used here does not work. The reason for this behaviour was not further investigated but could originate from competitive effects with e.g. Fe(II), which were not considered in the modelling. The Co(II) isotherm on the BGP-1-C11 sample covers only the higher concentration range (Fig. 5-2b). The experimental data is within the uncertainty range of the modelling but is generally slightly underpredicted.

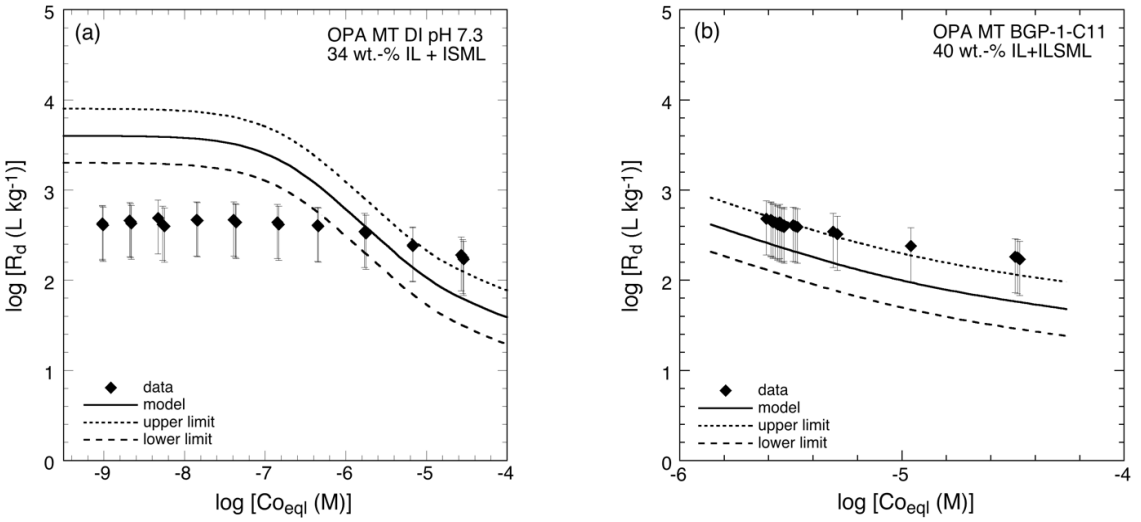

Fig. 5-2: Sorption measurements and modelling for Co(II) on Mont Terri Opalinus Clay samples (a) DI-A0-3.2 at pH = 7.3 (data taken from Baeyens et al. 2014) and (b) BGP-1-C11 at pH = 7.8

Data taken from Bradbury & Baeyens (2011)

5.1.2 Opalinus Clay from Schlattingen-1

Ni(II) and Co(II) isotherms were measured on an Opalinus Clay sample from the Schlattingen-1 borehole (SLA-938m). The mineralogical and porewater compositions are given in Tabs. 3-5 and 3-6, respectively.

The Ni(II) and Co(II) sorption isotherm are shown in Fig. 5-3. In the lower concentration range (< 10^{-6} M) the sorption of Ni(II) is slightly underestimated by ~ 0.5 log units. For Co(II), the experimentally covered low concentration range is small, however, the model prediction seems to slightly overpredict the sorption. At higher concentrations (> 10^{-6} M), the underprediction becomes more important (increasing uptake) for both elements, and the experimental data do not follow the shape of the model curve, as observed previously for Ni(II) on the Mont Terri sample at pH 8. As mentioned before, the reason for the increased sorption in the higher [Ni_{eql}] range is likely due to newly formed surface associated solids (see Section 5.6), which cannot be described by an adsorption equilibrium reaction.

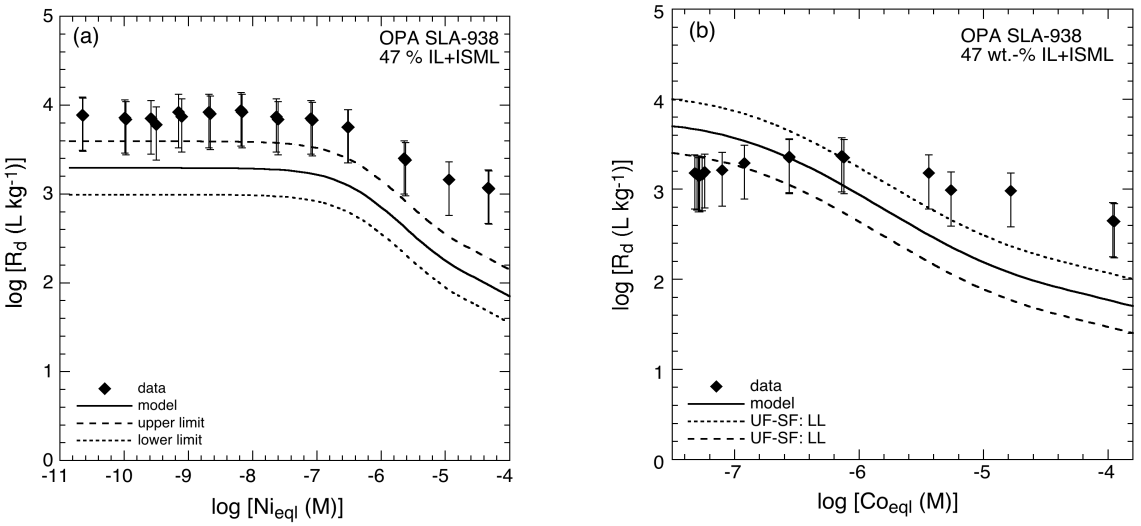

Fig. 5-3: Sorption measurements and modelling for (a) Ni(II) and (b) Co(II) on Opalinus Clay sample SLA-938 from the Schlattingen-1 borehole

Data taken from Baeyens et al. (2014)

5.2 Ni(II) and Co(II) isotherms on «Brauner Dogger» samples

The experimental data and modelling of Ni(II) and Co(II) sorption on the two «Brauner Dogger» samples with different clay contents are illustrated in Figs. 5-4 and 5-5, respectively. Mineralogy and porewater compositions are given in Tabs. 3-7 to 3-10.

In both cases, Ni(II) and Co(II) show similar sorption behaviour and the different clay content of the rock samples is reflected by the comparatively lower sorption in SLA-795. The blind predictions for Ni(II) and Co(II) on the «Brauner Dogger» samples (Figs. 5-4 and 5.5) describe the experimental data reasonably well in the low concentration ranges and the predictions for both metals lie within the experimental error bars. It should be noted that in the case of the clay-poor sample (Fig. 5-5) the predictions are quite good, illustrating that even for calcite-rich rocks (85% in the case of SLA-795) the bottom-up approach can be applied.

On the other hand, at equilibrium concentrations above ~ 10^{-6} M, the mismatch between experimental data and modelling becomes more significant (> 1 log unit) with increasing concentrations. To quantitatively describe the shape of the isotherms, additional surface sites could for example be considered; however, as will be shown later in this chapter and as mentioned previously, adsorption is probably no longer the mechanism controlling the retention in the higher concentration range. For the particular case of the safety assessment, the underprediction represents a pessimistic estimate.

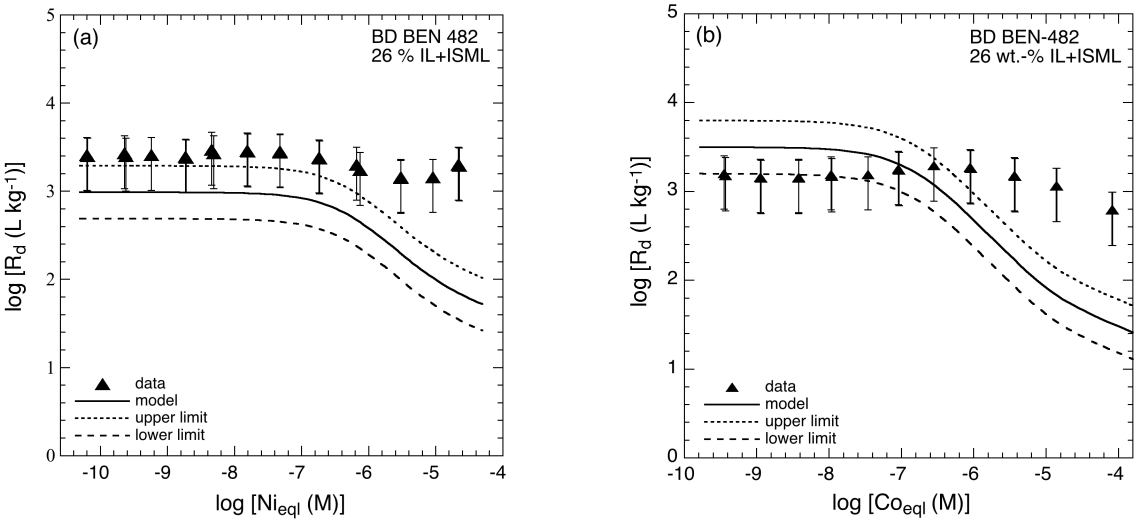

Fig. 5-4: Sorption measurements and modelling for (a) Ni(II) and (b) Co(II) on «Brauner Dogger» clay-rich sequences (sample BEN-482)

Data taken from Baeyens et al. (2014)

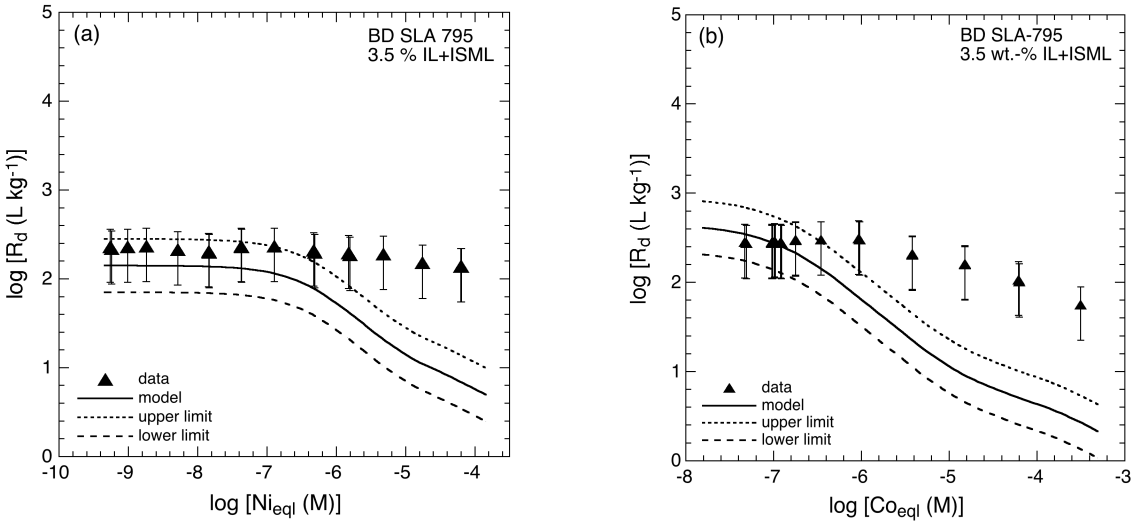

Fig. 5-5: Sorption measurements and modelling for (a) Ni(II) and (b) Co(II) on «Brauner Dogger» sandy limestone sequences (sample SLA-795)

Data taken from Baeyens et al. (2014)

5.3 Ni(II) and Co(II) isotherms on Effingen Member formation

The sorption of Ni(II) and Co(II) on two Effingen Member samples (differing by their clay content) and the corresponding blind predictions are illustrated in Figs. 5-6 and 5-7, respectively. Mineralogy and porewater compositions are given in Tabs. 3-11 to 3-14.

On the clay-richer samples (OFT-619; Figs. 5-6a and 5.6b), the blind predictions overestimate the sorption of Ni(II) and Co(II) (max. 0.7 log units) in the low concentration range (< 10^{-6} M). In the higher cation concentration range, the model re-produces the experimental data within the uncertainty range for Ni(II), the anomalous behaviour observed at higher divalent metal concentrations for other samples seems to be absent or less pronounced. For Co(II), adsorption is overpredicted, as observed previously.

On the clay-poorer samples (OFT-492) in the low concentration range (Figs. 5-7a and 5.7b), the model slightly underpredicts the experimental data for Ni (max. by 0.25 log units). Unfortunately, the experimental Co(II) data does not sufficiently cover the low concentration range to make a reliable statement, however, the existing data seems to suggest similar underprediction as for Ni. In the higher cation concentration range, the experimental data is well re-produced for Ni, as also observed for OFT-619. For Co(II), the blind prediction considerably overpredicts the sorption (up to 1.2 log units). On both clays, in the higher [Co_{eql}] range, Co sorption increasingly deviates from the blind prediction and the data cannot be modelled with the 2SPNE SC/CE model.

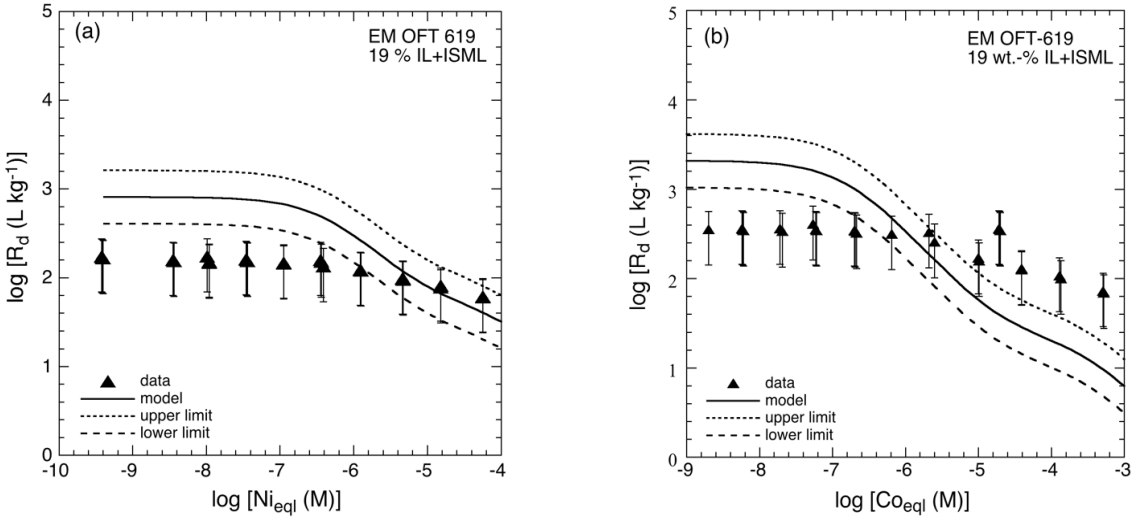

Fig. 5-6: Sorption measurements and modelling for (a) Ni(II) and (b) Co(II) on Effingen Member calcareous marl sequences (sample OFT-619)

Data taken from Baeyens et al. (2014)

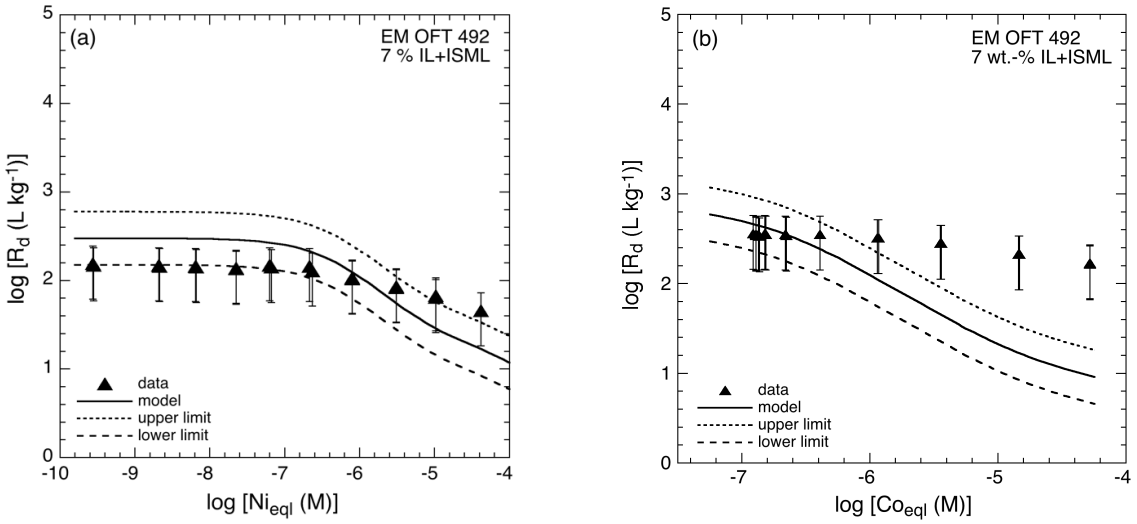

Fig. 5-7: Sorption measurements and modelling for (a) Ni(II) and (b) Co(II) for Effingen Member limestone sequences (sample OFT-492)

Data taken from Baeyens et al. (2014)

5.4 Ni(II) and Co(II) isotherms on Helvetic Marl

The Ni(II) isotherm measured on the Helvetic Marl from Wellenberg over a small concentration range (5×10^{-9} to 10^{-7} M) and the corresponding modelling results are depicted in Fig. 5-8a. The blind prediction overestimates the sorption by ~ 0.7 log units, and the data are outside the assumed model uncertainty range.

The Co(II) isotherm measured on the same Wellenberg sample covers a much larger concentration range. The results of the measurements and modelling are shown in Fig. 5-8b. In the lower [Co_{eql}] ($< 5 \times 10^{-7}$ M), the model and experimental data agree fairly well. At [Co_{eql}] $> 5 \times 10^{-7}$ M, however, the difference between the blind prediction and the experimental data is significant (up to 1.8 log units). The underprediction and concentration range (10^{-6} – 10^{-5} M) where the deviation occurs is, however, consistent with the previous observations.

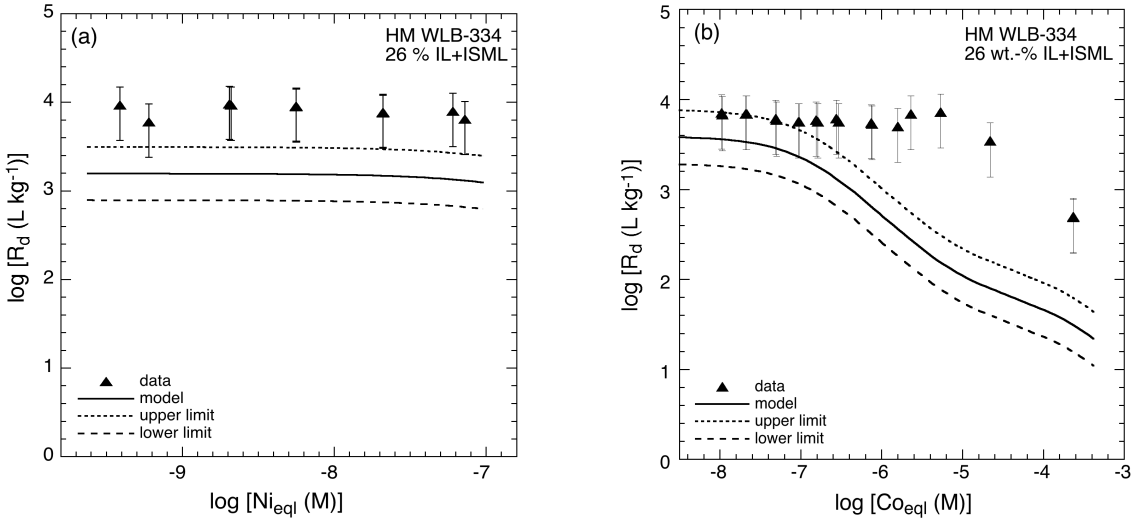

Fig. 5-8: Sorption measurements and modelling for (a) Ni(II) and (b) Co(II) on Helvetic Marl sample WLB-334

Data taken from Baeyens et al. (2014)

5.5 Ni(II) and Co(II) isotherms on non-Swiss argillaceous rocks

Ni(II) and Co(II) isotherms were measured on two different BCS samples (Ib-4 and delta-11; Tab. 3-17) in the same porewater (Tab. 3-18). The data on Ib-4 are from Marques Fernandes et al. (2015) whereas the data on delta-11 are unpublished PSI internal data (see Appendix A for the experimental details).

The experimental and modelling results for Ni(II) and Co(II) on the Ib-4 sample are shown in Figs. 5-9a and 5.9b, respectively. The blind predictions for $[Ni_{eql}] < 10^{-7}$ M and over the entire concentration range for Co are quite well (within the experimental error bars). As systematically observed for Ni(II) and Co(II) in the previous sections, the high $[Ni_{eql}]$ range is underestimated and cannot be modelled by the SCCs on the weak sites.

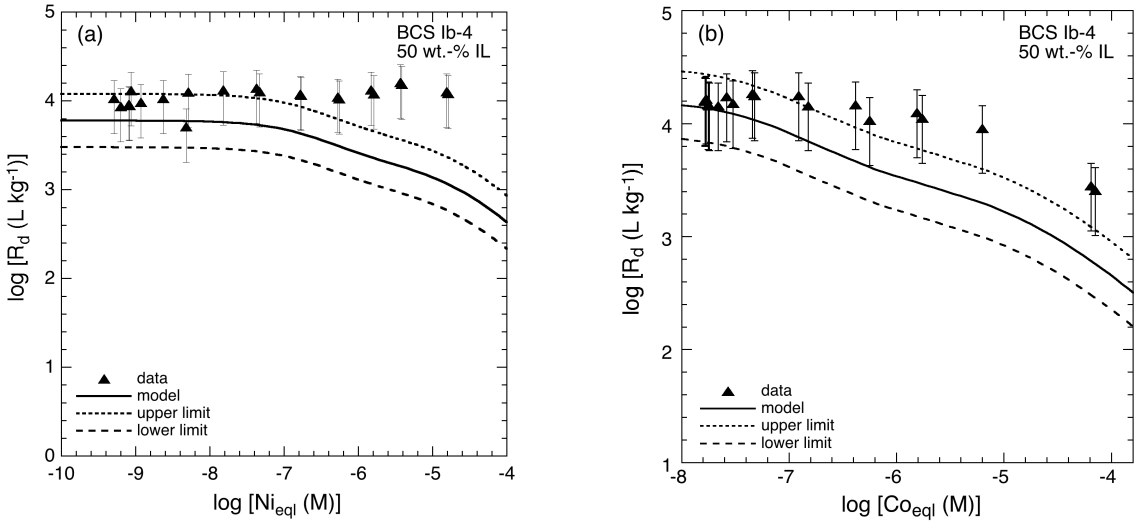

Fig. 5-9: Sorption measurements and modelling for (a) Ni(II) and (b) Co(II) on the BCS Ib-4 sample

Data taken from Marques Fernandes et al. (2015)

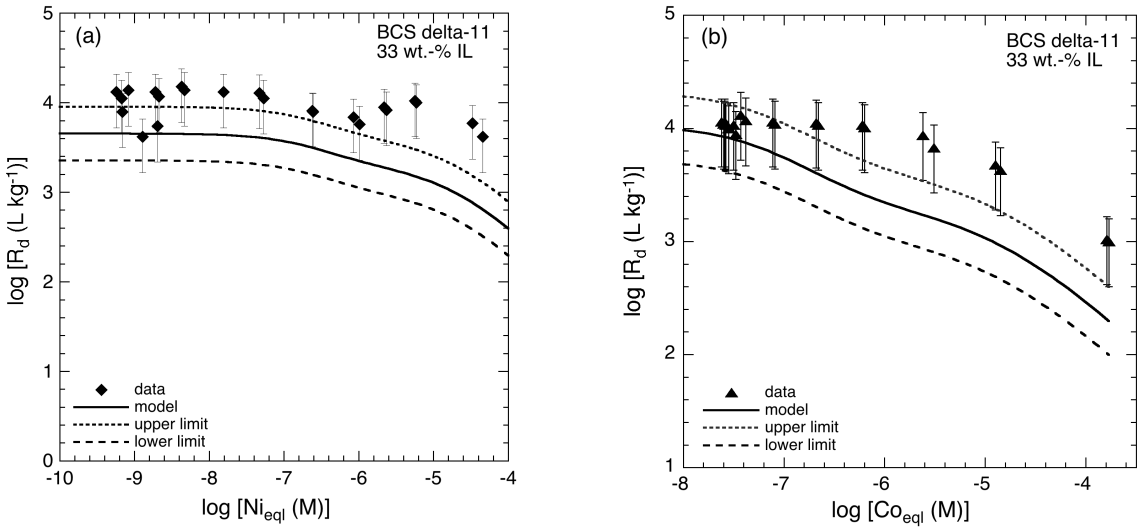

Fig. 5-10: Sorption measurements and modelling for (a) Ni(II) and (b) Co(II) on the BCS delta-11 sample

The results for Ni(II) and Co(II) on the delta-11 rock sample are shown in Figs. 5-10a and 5.10b, respectively. A similar observation can be made as for Ni(II) and Co(II) sorption on Ib-4., i.e. the experimental data for high [Ni_{eql}] cannot be predicted with the existing adsorption model. The sorption behaviour of Co(II) on both BCS samples is very similar.

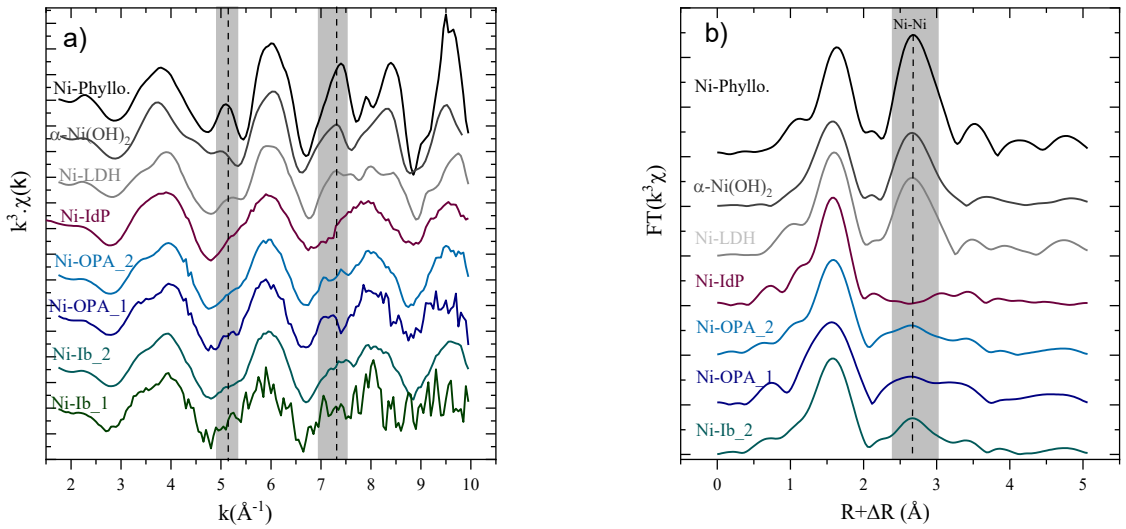

Fig. 5-11: (a) Raw k^3-weighted χ(k) spectra of Ni(II) sorbed onto Opalinus Clay and of Ni(II)-reference samples, and (b) the corresponding radial structure functions

Shaded areas indicate the appearance of distinct features arising from Ni-Ni single and multiple scattering interactions characteristic for specific Ni(II)-precipitates. Data are taken from Marques Fernandes et al. (2015).

5.6 Spectroscopic investigation

In case of the divalent transition metals Ni(II) and Co(II), the underestimation of most of the experimental data at higher equilibrium concentrations is systematic. The mismatch between the experimental data and modelling prediction at higher concentrations was addressed by Extended X-ray Absorption Fine Structure spectroscopy (EXAFS) in Marques Fernandes et al. (2015). Ni(II) loaded Boda Claystone (Ib) and Opalinus Clay (OPA) samples were prepared to cover the concentration region where model and experimental data diverge. EXAFS spectra were recorded for all samples along with three references: Ni(II) adsorbed on illite (IdP) (as a reference for a Ni(II) inner-sphere surface complex), Ni-layered double hydroxides (LDH) (taken from Scheinost & Sparks 2000) and Ni-phyllosilicate (taken from Ford et al. 1999; see also Fig. 5-11). The k^3 weighted $\chi(k)$-spectra of the two Ni-OPA samples are similar and exhibit distinct features at ~ 5.2 and 7.3 $Å^{-1}$, which are characteristic for Ni-solid phases (Scheinost and Sparks 2000). These features can be used as a fingerprint to discriminate adsorption from precipitation. The radial structure functions of Ni-OPA and Ni-Ib exhibit a backscattering contribution at 2.7 Å ($R + \Delta R$) originating from Ni-Ni interaction, typical for Ni-solid phases. The spectroscopic similarities of the Ni-OPA spectra with the Ni-solid phases and the difference with Ni-IdP suggest that the deviation between modelled and measured Ni-OPA and Ni-Ib isotherms is due to a surface induced precipitation of Ni solid phases. Chen et al. (2014) investigated the uptake of Ni(II) on COx. Their model satisfactorily estimates the Ni(II) sorption data on clay-rich COx. At higher Ni(II) loadings, in agreement with our observations, they also observed the neoformation of Ni(II) phyllosilicates with the help of EXAFS. In samples with lower clay mineral contents, however, they concluded that uptake by other minerals, especially by calcite, should not be neglected. It is well known that under given geochemical conditions (e.g. pH, metal concentrations), the sorption of Zn(II), Co(II), Ni(II) and Fe(II) can lead to the nucleation and precipitation of new phases such as hydroxides or phyllosilicates (e.g. Scheidegger et al. 1996, Scheinost et al. 1999, Ford & Sparks 2000, Dähn et al. 2002, Schlegel & Manceau 2006, Xu et al. 2018, Ford & Sparks 2000, Jacquat et al. 2008, Roberts et al. 1999, Zhu and Elzinga, 2014, Starcher et al. 2016, Zhang et al. 2019).

5.7 Summary

18 isotherms of Ni(II) and Co(II), out of 20 measured on the different rock samples, cover a large cation concentration range and two regions must be differentiated.

For the low Ni/Co concentration range ($< \sim 10^{-6}$ M), most data sets lie within the modelled uncertainty range or are close to the upper/lower limits of the model predictions. The sorption of Ni(II) on Opalinus Clay samples from Mont Terri (Fig. 5-2) and of Ni(II) and Co(II) on Effingen Member sample OFT-649 (Figs. 5-6a and 5.6b) is overestimated, concluding that in these cases the bottom-up approach cannot be applied despite both samples being rather clay-rich. There can be many reasons for this. One plausible reason could be competitive effects. The presence of other divalent cations in the natural rock system, which might compete with Ni/Co for adsorption on the strong sites, was not considered in this modelling exercise. Recently, it was shown that competitive sorption can considerably affect the uptake of trace metals (Marques Fernandes & Baeyens 2020).

In the higher concentration range ($\geq \sim 10^{-6}$ M), the majority of the data sets cannot be described by the 2SPNE SC/CE model. In all these cases, the uptake of Ni/Co is higher, likely due to the neoformation of Ni/Co phases as evidenced by spectroscopic measurements. The application of the bottom-up approach, however, would be conservative for the safety assessment for all these cases.

6 Europium

The present chapter summarises the experimental and modelling results for Eu(III) on the different rocks. The modelling approach is the same as used for Ni(II) and Co(II). The model, the associated parameters and the aqueous thermodynamic data for Eu(III) are summarised in Sections 2.2 and 2.3. The uncertainties for the model calculations are shown by the upper and lower limit curves according to the approach described in Section 2.4. The covered [Eu_{eql}] range is much narrower compared to Cs(I) and the divalent transition metals due to the much lower solubility of trivalent lanthanides in the synthetic porewater compositions. However, this concentration range largely covers the available pool of trivalent actinides and lanthanides in a high-level waste repository.

6.1 Eu(III) isotherms on Opalinus Clay

6.1.1 Mont Terri rock laboratory

Fig. 6-1 shows the Eu(III) sorption isotherms for Mont Terri Opalinus Clay sample BGP-1-C11 measured by Lauber et al. (2000) in two different porewaters (given in Tab. 3-2). The experimental data obtained in both porewaters at pH 6.3 and 8.0 are quite well described by the blind prediction.

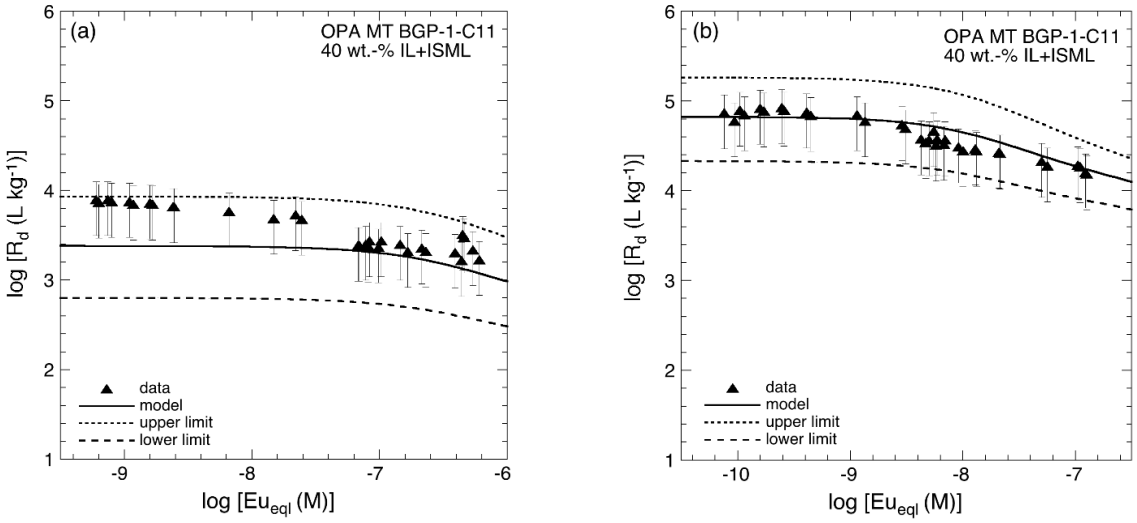

Fig. 6-1: Sorption measurements and modelling for Eu(III) on Mont Terri Opalinus Clay sample BGP-1-C11 at (a) pH 6.3 and (b) pH 8.0

Data taken from Lauber et al. (2000)

6.1.2 Schlattingen-1

Fig. 6-2 shows the Eu(III) sorption isotherm for Opalinus Clay from the Schlattingen-1 sample SLA-938. The blind predicted curve re-produces the experimental data quite well (within the assumed modelling uncertainty).

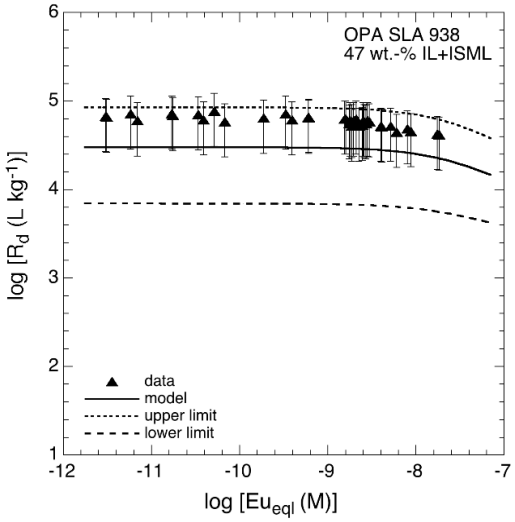

Fig. 6-2: Sorption measurements and modelling for Eu(III) on Opalinus Clay from the Schlattingen-1 sample SLA-938

Data taken from Marques Fernandes et al. (2015)

6.2 Eu(III) isotherms on 'Brauner' Dogger and Effingen Member formations

Eu(III) sorption isotherms were measured on the same confining unit samples as for the Cs(I), Ni(II) and Co(II) isotherms described in the previous chapters. The experimental measurements and modelling are shown for «Brauner Dogger» and Effingen Member in Figs. 6-3 and 6-4, respectively.

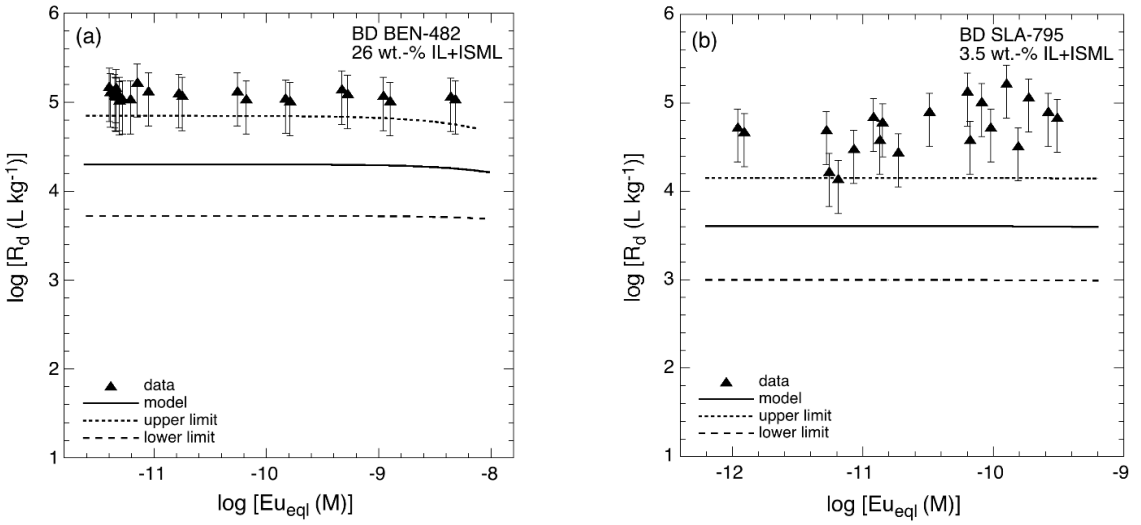

Fig. 6-3: Sorption measurements and modelling for Eu(III) on «Brauner Dogger» (a) clay-rich sequences (sample BEN-482) and (b) sandy limestone sequences (sample SLA-795)

Data taken from Baeyens et al. (2014)

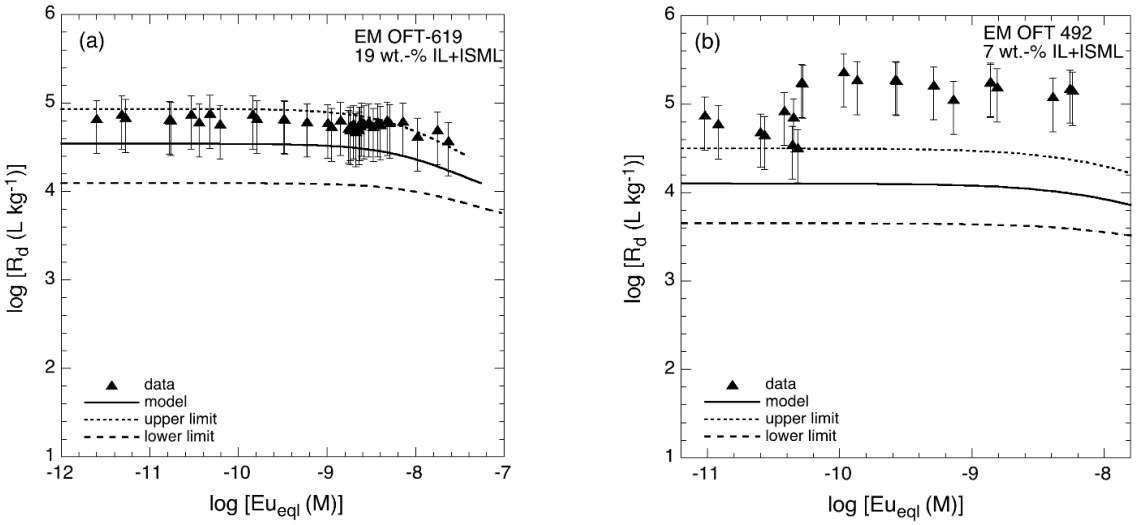

Fig. 6-4: Sorption measurements and modelling for Eu(III) on Effingen Member (a) calcareous marl sequences (sample OFT-619) and (b) limestone sequences (sample OFT-492)

Data taken from Baeyens et al. (2014)

For the samples with higher clay mineral contents (Figs. 6-3a and 6-4a), the blind prediction describes very well the obtained experimental data (OFT-619, Fig 6.4a) and slightly underpredicts the data on BEN-482 (Fig. 6-3a).

In contrary, the measured sorption of Eu(III) on the calcareous (clay-poor) samples are generally higher compared to the model calculations. In the modelling of the Eu(III) uptake, the assumption that only the 2:1 clay mineral content is responsible may not be valid if the carbonate mineral content becomes much more important than the clay mineral content, which is the case for the «Brauner Dogger» sample SLA-795 and Effingen Member sample OFT-492, with 2:1 clay mineral contents of 3.5 and 7 wt.-%, respectively. This may contribute to the larger discrepancies for these samples compared to the clay-rich samples. It can also be noticed that the scatter of the experimental data on these calcareous samples is much higher compared to the clay-rich samples. The enhanced sorption could be due to the formation of ternary Eu-carbonate surface complexes (Marques Fernandes et al. 2015) or/and due to the uptake of Eu(III) by calcite (Eu(III) is known to be strongly partitioned by calcite; Lakshtanov & Stipp 2004).

6.3 Eu(III) isotherms on Helvetic Marl

Only one Eu(III) isotherm was measured on the calcite-rich Helvetic Marl sample from Wellenberg (Baeyens et al. 2014) and the results of the measurements and modelling are illustrated in Fig. 6-5. Similar to the calcareous marl samples, the data are more scattered compared to the argillaceous rock samples and the sorption of Eu(III) is slightly underpredicted by the modelling (~ 0.8 log units). As in the previous case, the formation of ternary Eu-carbonate surface complexes or sorption on calcite could explain the higher sorption.

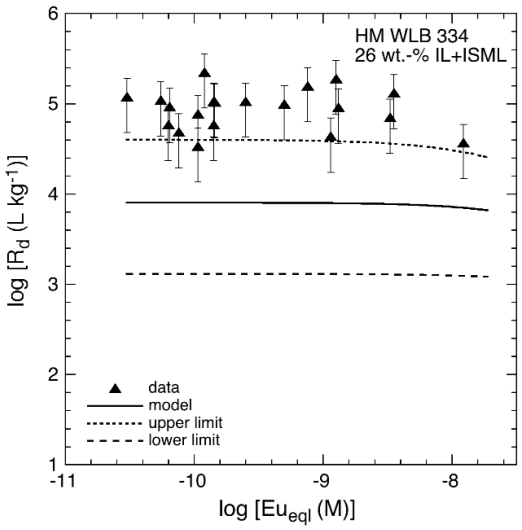

Fig. 6-5: Sorption measurements and modelling for Eu(III) on Helvetic Marl sample WLB-334

Data taken from Baeyens et al. (2014)

6.4 Eu(III) isotherms on non-Swiss argillaceous rocks

Eu(III) isotherms were measured on two different samples of BCS (lb-4 and delta-11). Experimental data and modelling on Ib-4 are taken from Marques Fernandes et al. (2015) and are shown in Fig. 6-6a. The unpublished PSI data on delta-11 and the respective modelling are shown in Fig. 6-6b. The experimental details for this sample are given in Appendix A. As in all previously shown cases the sorption is very high. The blind predicted curve re-produces the experimental data on Ib-4 well (within the assumed modelling uncertainty), whereas the sorption on delta-11 is slightly underestimated.

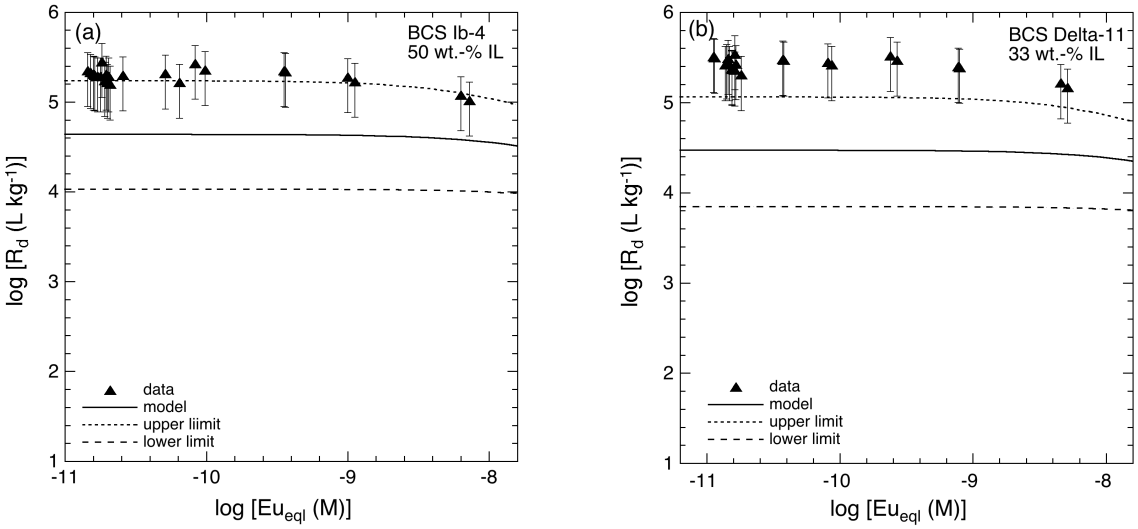

Fig. 6-6: Sorption measurements and modelling for Eu(III) on BCS samples (a) Ib-4 (Data taken from Marques Fernandes et al. (2015)) and (b) delta-11

6.5 Summary

Ten Eu(III) isotherms were measured on rock samples of Opalinus Clay, «Brauner Dogger», Effingen Member, marl and BCS. On all samples, the sorption of Eu(III) is very high and the data obtained on the calcareous samples scatter more (Figs. 6-3b, 6-4b and 6-5b). The sorption of Eu(III) on Opalinus Clay (Figs. 6-1a, 6-1b and 6-2) and on the Effingen Member sample OFT-619 is very well re-produced with 2SPNE SC/CE model developed for Eu(III) on illite, although the OFT-619 sample is mainly calcareous. The model calculations for the clay-rich sequences of «Brauner Dogger» (Fig. 6-3a) and BCS (Fig. 6-6) slightly underpredict the sorption of Eu(III), however, the experimental data overlap with the upper limit results of the modelling. The largest deviation between blind prediction and experimental data is observed for Eu(III) on the calcareous and clay-poor sandy limestone sequences of «Brauner Dogger» and limestone sequences of Effingen Member (Figs. 6-3b and 6-4b). In these carbonate-rich rocks, the uptake of Eu(III) by calcite (adsorption, incorporation) is likely to contribute to the high sorption (Lakshtanov & Stipp 2004). A general observation is that the model calculations for Eu(III) never overestimate the experimental data and therefore the use of the bottom-up approach for the safety assessment will be conservative.

7 Thorium

This chapter summarises the experimental and modelling results obtained for Th(IV) on the different rocks. The model, associated parameters and aqueous thermodynamic data for Th are summarised in Sections 2.2 and 2.3. Blind predictions were made by using the SCCs as derived in Bradbury & Baeyens (2017) and given in Tab. 2-4 (solid curves in figures in this Chapter 7).

For the Th(IV) isotherms, the covered concentration range is extremely small compared to Ni(II), Co(II) and Eu(III) due to the extremely low solubility of tetravalent actinides. Due to the low solubility, there are no SCCs for the weak sites.

7.1 Th(IV) isotherms on Opalinus Clay

7.1.1 Mont Terri rock laboratory

Fig. 7-1 shows the Th(IV) sorption isotherms on Mont Terri Opalinus Clay sample BGP-1-C11 measured in two different porewaters (see Tab. 3-2). The model calculations for Th(IV), shown by the solid lines in Fig. 7-1, either overpredict (Fig. 7-1a) or underpredict (Fig. 7-1b) the experimental data by ~ ± 0.3 log units. In the case that the pH is low and pCO_2 is high (Fig. 7-1a) the non-sorbing $Th(CO_3)_2(OH)_2^{2-}$ complex influences the calculated R_d values by ~ ± 0.5 log units. As shown in Tab. 2-8, the aqueous speciation is dominated by this ternary complex. For all other porewater compositions, the presence of this complex is less pronounced and hence the uncertainty range becomes small. See also the discussion in Section 2.4.2.2 where the effect of aqueous speciation for Th(IV) is illustrated in Fig. 2-1.

The calculated decrease of sorption at higher [Th_{eql}] is due to strong site saturation. Th(IV) uptake on the weak sites is not considered in the 2SPNE SC/CE model because of solubility constraints.

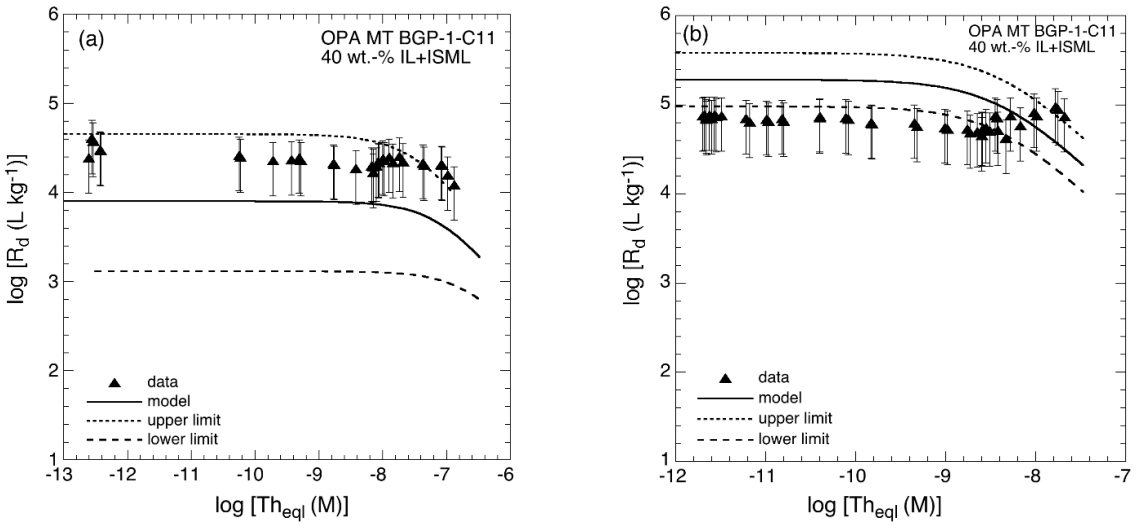

Fig. 7-1: Sorption measurements and modelling for Th(IV) on Mont Terri Opalinus Clay sample BGP-1-C11 at (a) pH 6.3 and (b) pH 7.8

Data taken from Lauber et al. (2000)

7.1.2 Schlattingen-1

Fig. 7-2 shows the Th(IV) sorption isotherm on Opalinus Clay sample SLA-938. The data is taken from Marques Fernandes et al. (2015). Similar to the Opalinus Clay sample from Mont Terri, the blind prediction is acceptable and the error bars of the data overlap with the lower limit modelling uncertainty range.

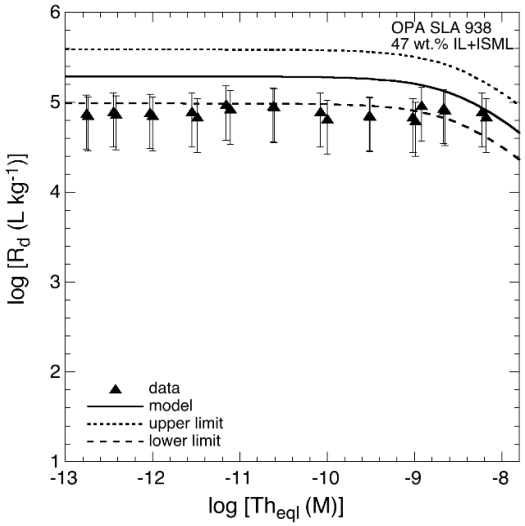

Fig. 7-2: Sorption measurements and modelling for Th(IV) on Opalinus Clay from the Schlattingen-1 borehole (sample SLA-938)

Data taken from Marques Fernandes et al. (2015)

7.2 Th(IV) isotherms on «Brauner Dogger» and Effingen Member formations

The experimental data and modelling for Th(IV) on «Brauner Dogger» and Effingen Member samples are shown in Figs. 7-3 and 7-4, respectively. The blind predictions for three of the rock samples are in a very good agreement with the experimental data. Only in the case of the «Brauner Dogger» clay-rich sequences (sample BEN-482; Fig. 7-3a), the blind prediction slightly overestimates the experimental data by 0.3 log units. However, the blind prediction for Th(IV) can be regarded as very good considering the different mineralogical nature and 2:1 clay mineral content varying from 3.5 to 26 wt.-% for these rock samples.

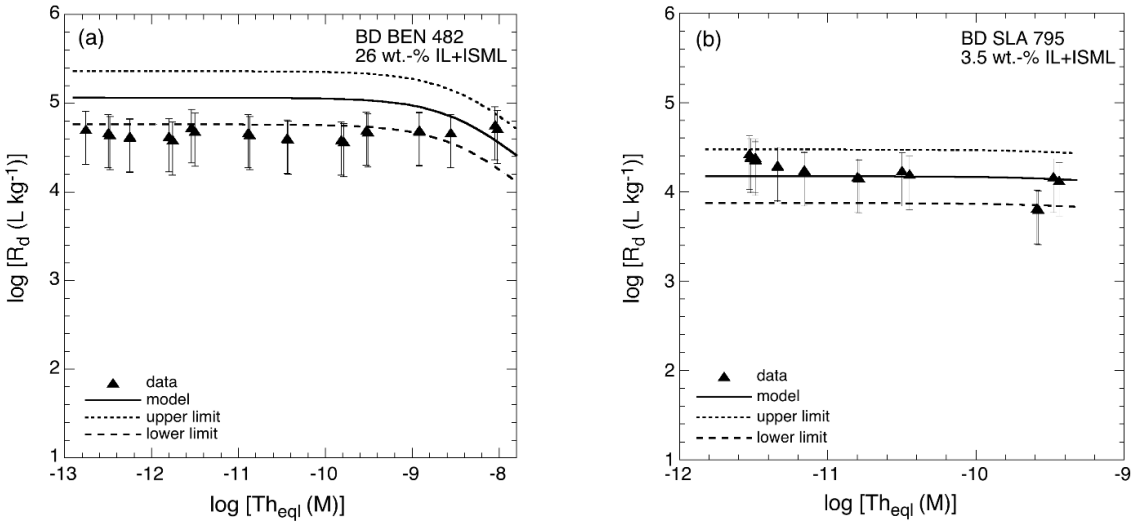

Fig. 7-3: Sorption measurements and modelling for Th(IV) on «Brauner Dogger» (a) clay-rich sequences (sample BEN-482) and (b) sandy limestone sequences (sample SLA-795)

Data taken from Baeyens et al. (2014)

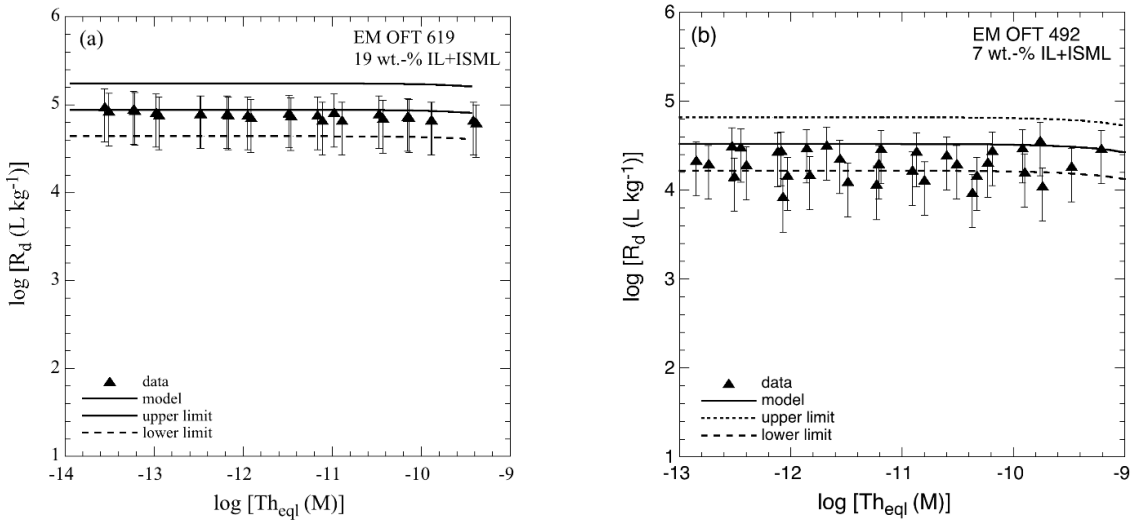

Fig. 7-4: Sorption measurements and modelling for Th(IV) on Effingen Member (a) calcareous marl sequences (sample OFT-619) and (b) limestone sequences (sample OFT-492)

Data taken from Baeyens et al. (2014)

7.3 Th(IV) isotherms on Helvetic Marl

The Th(IV) isotherm measured on the Helvetic Marl sample WLB-334 from Wellenberg and the the corresponding modelling are shown in Fig. 7-5. The blind prediction slightly underestimates (by ~ 0.4 log units) the experimental data, but the data are within the modelling uncertainty range.

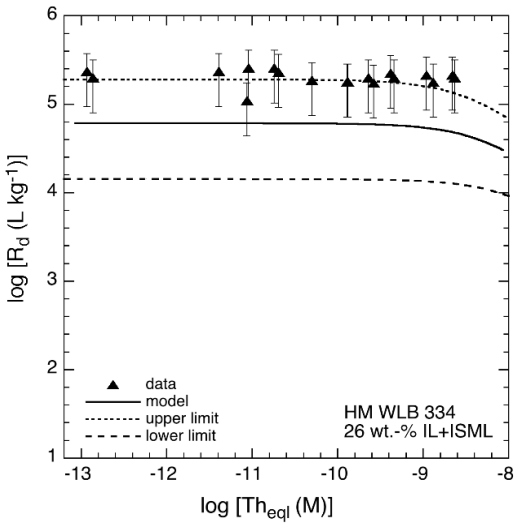

Fig. 7-5: Sorption measurements and modelling for Th(IV) on Helvetic Marl sample WLB-334

Data taken from Baeyens et al. (2014)

7.4 Th(IV) isotherms on non-Swiss argillaceous rocks

Th(IV) isotherms were measured on two different BCS samples (lb-4 and delta-11). Data on Ib-4 are taken from Marques Fernandes et al. (2015), whereas the data on delta-11 are unpublished PSI data (see Appendix A). The results of the measurements and modelling are shown in Figs. 7-6a and 7-6b, respectively. The blind predictions slightly underestimate the sorption on Ib-4 by ~ 0.4 log units and on delta-11 by ~ 0.7 log units.

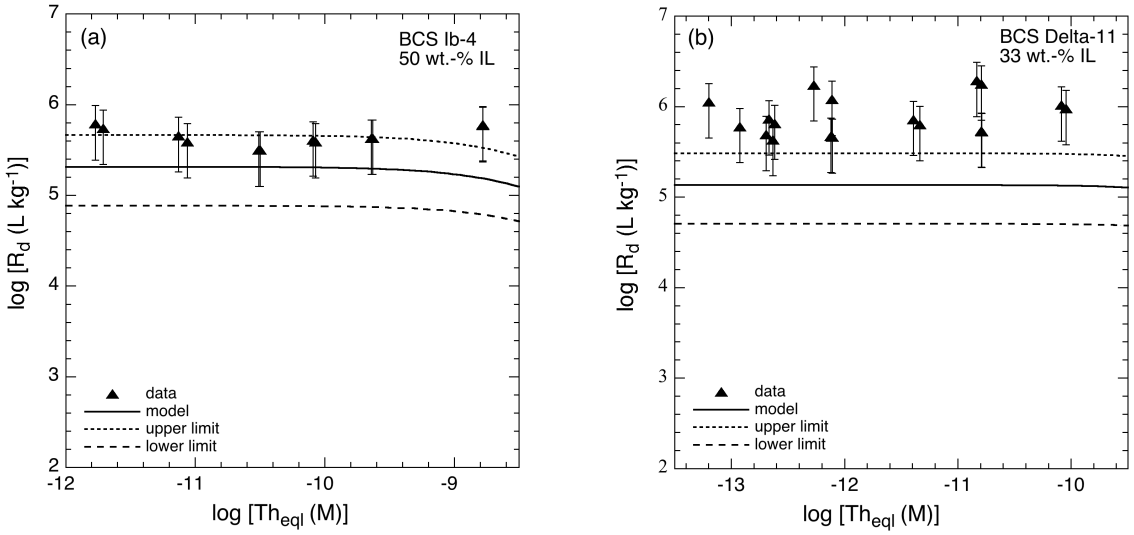

Fig. 7-6: Sorption measurements and modelling for Th(IV) on the BCS samples (a) Ib-4 (Data taken from Baeyens et al. (2014)) and (b) delta-11

7.5 Summary

In general, the sorption of Th(IV) on all rock samples is comparatively high and little affected by the synthetic porewater composition except for the high pCO_2 porewater (Mont Terri Opalinus Clay sample BGP-1-C11 at pH 6.3), in agreement with an influence of the aqueous speciation. The agreement between the blind predicted adsorption and the experimental data is in most cases quite well, even for the clay-poorest sample («Brauner Dogger» sandy limestone sequences sample SLA-795).

8 Uranyl

The experimental data and the predictive modelling results for U(VI) on the different rocks are given below. The same modelling approach as for Ni(II), Co(II), Eu(III) and Th(IV) was applied. The 2 SPNE CE/SC model parameters and aqueous thermodynamic data for U(VI) are summarised in Sections 2.2 and 2.3. The different porewaters and mineralogical compositions of the rock samples are given in Chapter 3. The model uncertainty range on the modelling originating from the uncertainty estimate on the strong site capacity and on the dominant aqueous complexes are illustrated by the dotted and dashed curves in figures in this chapter.

8.1 U(VI) isotherms on Opalinus Clay

U(VI) sorption isotherms on Opalinus Clay samples from Mont Terri (BGP-1-C11) and Schlattingen-1 (SLA-938) at pH ~ 8 in the corresponding porewaters are shown in Fig. 8-1a and 8.1b, respectively. The experimental data were taken from Baeyens et al. (2014) and Marques Fernandes et al. (2015), respectively. The model calculations of U(VI) adsorption on both Opalinus Clay samples describe the experimental data very well, despite the considerable decrease in sorption attributable to the formation of strong U-carbonato species.

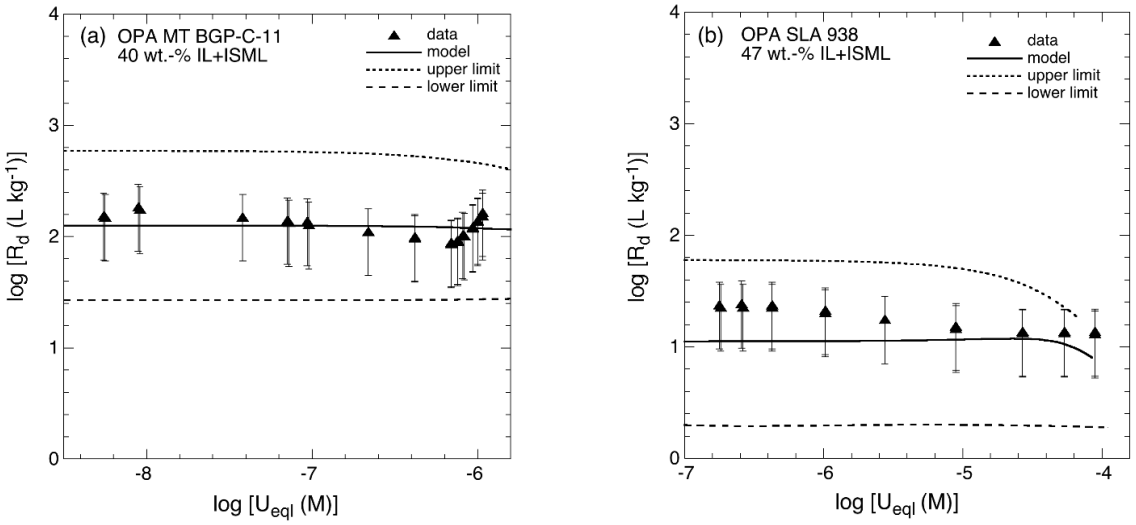

Fig. 8-1: Sorption measurements and modelling for U(VI) sorption on Opalinus Clay samples from (a) Mont Terri (BGP-1-C11) (data taken from Baeyens et al. 2014) and (b) Schlattingen-1 (SLA-938)

Data taken from Marques Fernandes et al. (2015)

8.2 U(VI) isotherms on «Brauner Dogger» and Effingen Member formations

Experimental and modelling data for U(VI) for «Brauner Dogger» and Effingen Member samples are shown in Figs. 8-2 and 8-3, respectively. All experimental data are taken from Baeyens et al. (2014).

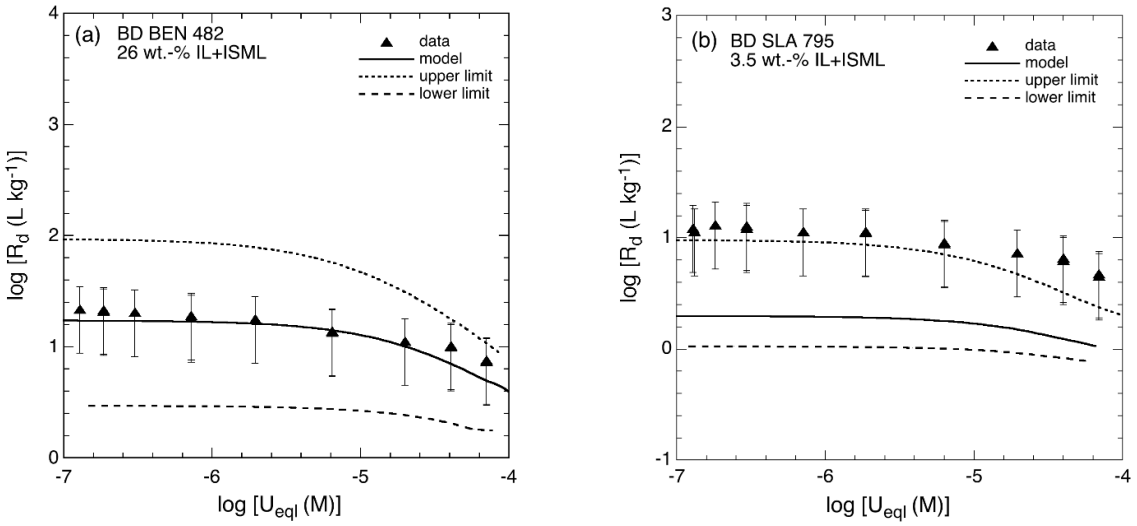

Fig. 8-2: Sorption measurements and modelling for U(VI) on «Brauner Dogger» (a) clay-rich sequences (sample BEN-482) and (b) sandy limestone sequences (sample SLA-795)

Data taken from Baeyens et al. (2014)

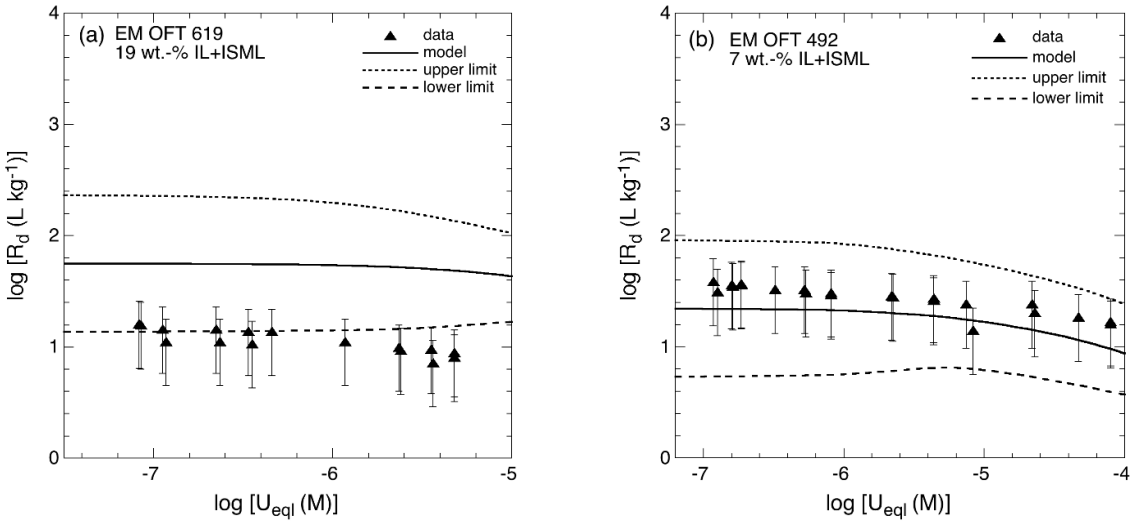

Fig. 8-3: Sorption measurements and modelling for U(VI) on Effingen Member (a) calcareous marl sequences (sample OFT-619) and (b) limestone sequences (sample OFT-492)

Data taken from Baeyens et al. (2014)

The adsorption of U(VI) on the «Brauner Dogger» clay-rich sequences (Fig. 8-2a) and the Effingen Member clay-poor limestone sequences (Fig. 8-3b) is very well described by the bottom-up approach.

The blind predictions of U(VI) on the «Brauner Dogger» sandy limestone sequences (Fig. 8-2b) and the Effingen Member calcareous marl sequences (Fig. 8-3a) slightly under- or overestimate the experimental data by max. 0.7 log units. However, in both cases, the experimental data lie within the uncertainty range of the modelling approach.

8.3 U(VI) isotherm on Helvetic Marl

An U(VI) isotherm was measured on Helvetic Marl sample WLB-334 originating from Wellenberg (Baeyens et al. 2014) and the results of the measurements and modelling are shown in Fig. 8-4. The blind prediction for this system deviates significantly from the measured U(VI) sorption isotherm (up to 1.4 log units). The reason for the underestimation of the model calculations at low [U_{eql}] is not understood.

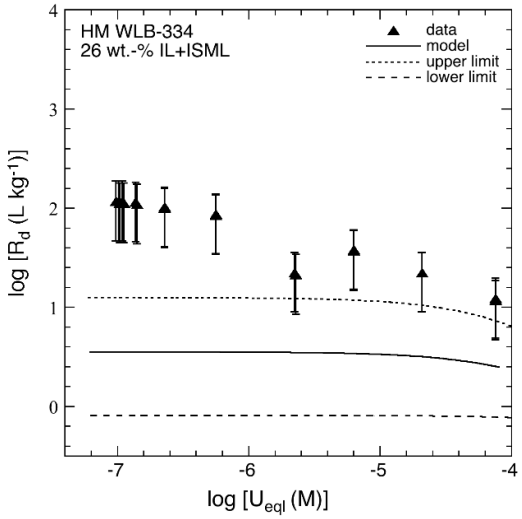

Fig. 8-4: Sorption measurements and modelling for U(VI) on Helvetic Marl sample WLB-334
Data taken from Baeyens et al. (2014)

8.4 U(VI) isotherm on non-Swiss argillaceous rocks

The U(VI) isotherm measured on BCS sample Ib-4 (Marques Fernandes et al. 2015) is shown in Fig. 8-5. The model calculation shows a good agreement with the experimental results.

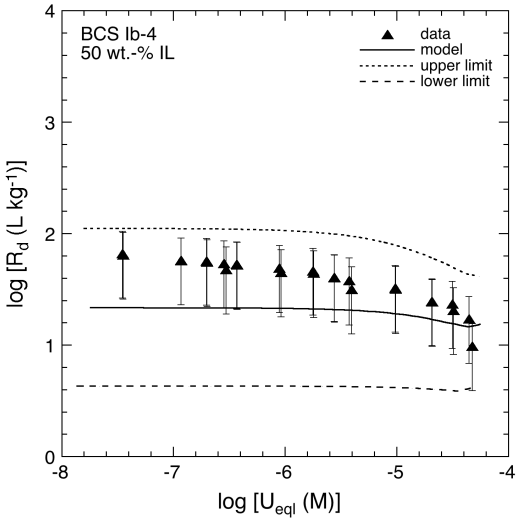

Fig. 8-5: Sorption measurements and modelling for U(VI) on the BCS sample Ib-4
Data taken from Marques Fernandes et al. (2015)

8.5 Summary

In the eight porewaters used for the U(VI) isotherms, the U(VI) speciation is dominated by the complexation with carbonate species (see Tab. 2-8). Less than 1% of U(VI) is hydrolysed, which is reflected by the strongly decreased sorption. Nevertheless, the blind predictions for U(VI) sorption on natural rock samples is in most cases, except for the isotherm on Helvetic Marl (Fig. 8-5), very satisfactory. There is a clear overlap between the model calculations and the experimental data considering the uncertainty ranges for both.

9 Conclusions

Reliably predicting the long-term fate of (radio-)contaminants under realistic geochemical conditions is a key issue in the safety assessment of a deep geological repository for radioactive waste. Sorption on rocks from geological formations envisaged as potential host rocks in Switzerland and in many other countries is by nature too complex to be easily predicted and the parameterisation of the necessary sorption models is very challenging given the multi-mineral composition of these rocks. In the case of argillaceous rocks, this modelling task can be considerably simplified by considering 2:1 clay minerals as the preferential sorbents, based on their high sorption properties. However, under this assumption, it is crucial to understand the adsorption processes on pure clay minerals and to develop robust thermodynamic sorption models able to predict the adsorption processes reliably under realistic geochemical conditions.

The present report aims at testing the capabilities of two developed adsorption models for illite, (i) the generalised Cs sorption (GCS) model and (ii) the 2 Site Protolysis Non Electrostatic Surface Complexation and Cation Exchange (2SPNE SC/CE) model, together with their associated parameters, to blind predict sorption isotherms of Cs(I), Ni(II), Co(II), Eu(III), Th(IV) and U(VI) measured on different rocks (with different clay mineral contents). Blind predictions were made by applying the appropriate sorption model for the respective element on illite, scaled to the 2:1 clay mineral or illite content and by considering the aqueous speciation of the element in the respective porewater. It should be noted that the models were developed on a very specific illite (Illite du Puy) and not on the illite extracted from the rock samples, which might slightly differ in their sorption characteristic (i.e., site capacities).

For the safety assessment of the general licence application as part of the Swiss disposal programme, state-of-the-art sorption databases will have to be provided. It is foreseen to calculate the different sorption databases by using the bottom-up approach. The methodology will allow to calculate the R_d values directly, considering the aqueous speciation, adsorption competition, solubility limits and concentration-dependent adsorption of each radionuclide for each specific rock-porewater system. The verification and validation of the bottom-up approach to justify its applicability in the context of the important upcoming safety assessment is therefore essential.

For Cs(I), the modelling re-produced most of the isotherms very well. The maximum deviation between blind prediction and experimental data was observed for the transition metals Co(II) and Ni(II), particularly in the higher equilibrium concentration range. The blind predictions for Co(II) and Ni(II) on the different rock samples deviated at the maximum by 1 log unit in the lower metal equilibrium concentration range (*i.e.* range where the surface speciation is dominated by the strong sites). In two cases, the sorption is overestimated, despite both samples being rather clay rich. One possible explanation could be the ubiquitous presence of divalent cations (*i.e.*, Fe(II), Mn(II)) in the natural rock system, competing with Ni(II) for adsorption on the strong sites. A recent study showed that competitive sorption between divalent cations considerably affects the uptake of trace metals (Marques Fernandes & Baeyens 2020). In the development of the SDB for the general licence application, competitive sorption will be considered. A major contribution of calcite in the retention of divalent cations could not be confirmed in this study.

At metal equilibrium concentrations $< 10^{-6}$ M the calculations clearly underestimate the sorption for both metals on most of the rock samples. The reason for the discrepancy between modelling and experimental results at higher equilibrium concentrations is likely the formation of surface precipitates as confirmed by Ni EXAFS measurements on Opalinus Clay and Boda Claystone samples. The sorption modelling approach does not consider the formation of precipitates, implying that in environments where the uptake of metals is governed by such uptake processes

the 2SPNE SC/CE model is no longer applicable. For the safety assessment, this process leading to an enhanced uptake of divalent transition metals would be beneficial. However, such a process is not expected to take place under "in situ" conditions since such high radionuclide releases are not anticipated in the far field of a high-level waste repository.

Eu(III) sorption isotherms for almost all rocks are systematically slightly underestimated, even so the general prediction is rather good with a maximum deviation from the experimental data of one order of magnitude. The enhanced sorption could be due to the formation of ternary Eu-carbonate surface complexes, not considered in the modelling, and/or by the partitioning of Eu(III) into calcite.

For Th(IV) the blind predictions re-produce the experimental data well. The modelled curves for most rocks lie within or just above/below the uncertainty range, with a maximum deviation of ~ 0.7 log units.

For the case of U(VI), the blind predictions are mostly good except for Helvetic Marl (highest carbonate concentration), with a maximum deviation of ~ 1.2 log units. It should be underlined that the importance of aqueous carbonate complexes, and particularly the ternary uranyl-calcium-carbonate complexes, have a large influence on the sorption of U(VI) since they form strong complexes, which are considered to be non-sorbing. However, it is anticipated that after closure of the repository, reducing conditions will prevail in the near field. Under such conditions U(IV) will be the dominant species, which forms less strong carbonato complexes and behaves similar to Th(IV).

In view of the uncertainties related to the complexity of the natural rocks and to the thermodynamic sorption modelling, it can be concluded that the simplified bottom-up approach provides a fairly good blind prediction tool for the absorption of a series of metals (oxidation states from I to IV and VI) on different sedimentary rocks.

Consequently, this approach and the underlying sorption models can be used to describe the uptake of Cs(I), Co(II), Ni(II), Eu(III), Th(IV) and U(VI) in geological formations providing that adsorption on 2:1 clay minerals is the dominant retention mechanism. In clay-poor rocks, other minerals, especially calcite, might control the retention of metals.

For the safety assessment supporting the general licence application in Switzerland, the bottom-up approach presented in this report will be applied, where appropriate, for the derivation of SDBs for argillaceous host rocks and buffer material. A total of sixty-four sorption isotherms, comprising five different radionuclides, fifteen different rock types (clay-rich/clay-poor) and 16 different porewater compositions, have been compiled and modelled using the bottom-up approach. Generally, in most cases, the blind predictions describe the sorption measurements well. In the cases where the model underpredicts the experimental data because of non-sorbing phenomena (e.g. surface precipitation) or experimental artefacts, the calculated R_d values can be regarded as conservative for the safety assessment. In three cases involving only divalent cations, the blind predictions overestimate the experimental sorption data (see Figs. 5-2, 5-6a and 5-6b), the reason for which is not clear. Competitive effects, in case they occur, can reduce the adsorption of the element considered and if not accounted for can lead to an overestimated prediction. In the derivation of the SDBs, competitive adsorption (e.g. between divalent metals) will be taken into account. It can be safely concluded that the results from this study contribute considerably to the confidence and robustness of the sorption databases that will be developed using the bottom-up approach towards sorption within the framework of future safety assessments.

Acknowledgements

We would like to thank Astrid Schaible and Vanessa Kalbermatter for technical assistance. Prof. Dr. V. Brendler (Helmholz-Zentrum Dresden-Rossendorf, Germany), Prof. Dr. B. Grambow (IMT Atlantique, Nantes, France) and Dr. S. Serno (Nagra, Switzerland) are gratefully acknowledged for reviewing the manuscript. Partial financial support was provided by Nagra.

10 References

Arnold, T., Zorn, T., Zänker, H., Bernhard, G. & Nitsche, H. (2001): Sorption behavior of U(VI) on phyllite: experiments and modeling. Journal Contam. Hydrol. 47, 219-231.

Ayoub, A., Pfingsten, W., Podofillini, L. & Sansavini, G. (2020): Uncertainty and sensitivity analysis of the chemistry of cesium sorption in deep geological repositoris. Applied Geochemistry 117, 104607.

Baeyens, B. (1982): Strontium, cesium and europium retention in Boom Clay: A potential repository site for nuclear waste, Faculty of Agronomy. Katholieke Universiteit Leuven, Leuven, Belgium.

Baeyens, B. & Bradbury, M.H. (1995): A quantitative mechanistic description of Ni, Zn and Ca sorption on Na-montmorillonite. Part II: Sorption measurements. PSI Bericht Nr. 95-11. Paul Scherrer Institute, Villigen PSI, Switzerland.

Baeyens, B. & Bradbury, M.H. (1997): A mechanistic description of Ni and Zn sorption on Na-montmorillonite. 1. Titration and sorption measurements. J. Contam. Hydrol. 27, 199-222.

Baeyens, B. & Bradbury, M.H. (2017): The development of a thermodynamic sorption database for montmorillonite and the application to bentonite. PSI Bericht Nr. 17-05 and Nagra Technical Report NTB 17-13.

Baeyens, B. & Marques Fernandes, M. (2018): 5 - Adsorption of heavy metals including radionuclides. *In:* Schoonheydt, R., Johnston, C.T. & Bergaya, F. (eds.): Developments in Clay Science. Elsevier, Amsterdam, The Netherlands, pp. 125-172.

Baeyens, B., Marques Fernandes, M. & Bradbury, M.H. (2014): Comparison of sorption measurements on argillaceous rocks and bentonite with predictions using the SGT-E2 approach to derive sorption data bases. Nagra Technical Report NTB 12-05.

Bradbury, M.H. & Baeyens, B. (1997): A mechanistic description of Ni and Zn sorption on Na-montmorillonite. 2. Modelling. J. Contam. Hydrol. 27, 223-248.

Bradbury, M.H. & Baeyens, B. (1998): A physicochemical characterisation and geochemical modelling approach for determining porewater chemistries in argillaceous rocks. Geochim. Cosmochim. Acta 62, 783-795.

Bradbury, M.H. & Baeyens, B. (2000): A generalised sorption model for the concentration dependent uptake of caesium by argillaceous rocks. Journal Contam. Hydrol. 42, 141-163.

Bradbury, M.H. & Baeyens, B. (2009a): Sorption modelling on illite Part I: Titration measurements and the sorption of Ni, Co, Eu and Sn. Geochim. Cosmochim. Acta 73, 990-1003.

Bradbury, M.H. & Baeyens, B. (2009b): Sorption modelling on illite. Part II: Actinide sorption and linear free energy relationships. Geochim. Cosmochim. Acta 73, 1004-1013.

Bradbury, M.H. & Baeyens, B. (2011): Predictive sorption modelling of Ni(II), Co(II), Eu(IIII), Th(IV) and U(VI) on MX-80 bentonite and Opalinus Clay: A bottom-up approach. Applied Clay Science 52, 27-33.

Bradbury, M.H. & Baeyens, B. (2017): The development of a thermodynamic sorption data base for illite and the application to argillaceous rocks. PSI Bericht Nr 17-06 and Nagra Technical Report NTB 17-14.

Breitner, D., Osan, J., Fabian, M., Zagyvai, P., Szabo, C., Dahn, R., Marques Fernandes, M., Sajo, I.E., Mathe, Z. & Torok, S. (2015): Characteristics of uranium uptake of Boda Claystone Formation as the candidate host rock of high level radioactive waste repository in Hungary. Environmental Earth Sciences 73, 209-219.

Brouwer, E., Baeyens, B., Maes, A. & Cremers, A. (1983): Cesium and rubidium ion equilibriums in illite clay. Journal of Physical Chemistry 87, 1213-1219.

Chen, Z., Montavon, G., Guo, Z., Wang, X., Razafindratsima, S., Robinet, J.C. & Landesman, C. (2014): Approaches to surface complexation modeling of Ni(II) on Callovo-Oxfordian clayrock. Applied Clay Science 101, 369-380.

Choppin, G.R. (1995): Comparative solution chemistry of the 4f and 5f elements. Journal of Alloys and Compounds 223, 174-179.

Davies, C.W. (1962): Ion association. Butterworths, Washington, D.C., USA.

Davis, J.A., Coston, J.A., Kent, D.B. & Fuller, C.C. (1998): Application of the surface complexation concept to complex mineral assemblages. Environmental Science & Technology 32, 2820-2828.

De Preter, P., Van Loon, L., Maes, A. & Cremers, A. (1991): Solid/liquid distribution of radiocesium in Boom Clay. A quantitative interpretation. Radiochim. Acta, 52/53, 299-302.

Ford, R.G., Scheinost, A.C., Scheckel, K.G. & Sparks, D.L. (1999): The link between clay mineral weathering and the stabilization of Ni surface precipitates. Environmental Science & Technology 33, 3140-3144.

Griffault, L., Merceron, T., Mossman, J.R., Neerdael, B., De Cannière, P., Beaucaire, C., Daumas, S., Bianchi, A. & Christen, R. (1996): Acquisition et regulation de la chimie des eaux en milieu argileux pour la projet de stockage de déchets radioactifs en formation géologique. Projet Archimède argile, Rapport final (EUR 17454). EC Publications, Luxembourg.

Grim, R.E. (1953): Clay Mineralogy. McGraw Hill, New York, NY, USA.

Lakshtanov, L.Z. & Stipp, S.L.S. (2004): Experimental study of europium (III) coprecipitation with calcite. Geochim. Cosmochim. Acta 68, 819-827.

Lauber, M., Baeyens, B. & Bradbury, M.H. (2000): Physico-chemical characterisation and sorption measurements of Cs, Sr, Ni, Eu, Th, Sn and Se on Opalinus Clay from Mont Terri. PSI Bericht Nr. 00-10 and Nagra Technical Report NTB 00-11.

Marques Fernandes, M. & Baeyens, B. (2020): Competitive adsorption on illite and montmorillonite: Experimental and modelling investigations. Nagra Technical Report NTB 19-05.

Marques Fernandes, M., Scheinost, A.C. & Baeyens, B. (2016): Sorption of trivalent lanthanides and actinides onto montmorillonite: Macroscopic, thermodynamic and structural evidence for ternary hydroxo and carbonato surface complexes on multiple sorption sites. Water Research 99, 74-82.

Marques Fernandes, M., Stumpf, T., Baeyens, B., Walther, C. & Bradbury, M.H. (2010): Spectroscopic identification of ternary Cm-carbonate surface complexes. Environmental Science & Technology 44, 921-927.

Marques Fernandes, M., Vér, N. & Baeyens, B. (2015): Predicting the uptake of Cs, Co, Ni, Eu, Th and U on argillaceous rocks using sorption models for illite. Applied Geochemistry 59, 189-199.

McKinley, I.G. & West, J.M. (1982): Sorption/desorption properties of argillaceous strata from boreholes at Harwell. Environmental Protection Unit. ENPU 82-6.

Melkior, T., Yahiaoui, S., Motellier, S., Thoby, D. & Tevissen, E. (2005): Cesium sorption and diffusion in Bure mudrock samples. Applied Clay Science 29, 172-186.

Miron, G.D., Kulik, D.A., Dmytrieva, S.V. & Wagner, T. (2015): GEMSFITS: Code package for optimization of geochemical model parameters and inverse modeling. Applied Geochemistry 55, 28-45.

Nagra (2002): Project Opalinus Clay: Safety Report. Demonstration of disposal feasibility (Entsorgungsnachweis) for spent fuel, vitrified high-level waste and long-lived intermediate-level waste. Nagra Technical Report NTB 02-05.

Neck, V. & Kim, J.I. (2001): Solubility and hydrolysis of tetravalent actinides. Radiochim. Acta 89, 1-16.

OECD/NEA (2012): Thermodynamic Sorption Modelling in Support of Radioactive Waste Disposal Safety Cases. NEA Sorption Project Phase III, OECD Publishing, Paris, https://doi.org/10.1787/9789264177826-en

Payne, T.E., Brendler, V., Ochs, M., Baeyens, B., Brown, P.L., Davis, J.A., Ekberg, C., Kulik, D.A., Missana, T., Tachi, Y., Van Loon, L.R. & Altmann, S. (2013): Guidelines for thermodynamic sorption modelling in the context of radioactive waste disposal. Environ. Model. Softw. 42, 143-156.

Pearson, F.J. (1998): Artificial waters for use in laboratory and field experiments with Opalinus Clay: Status June 1998. TM-44-98-08. Paul Scherrer Institute, Villigen PSI, Switzerland.

Savoye, S., Beaucaire, C., Fayette, A., Herbette, M. & Coelho, D. (2012): Mobility of cesium through the Callovo-Oxfordian claystones under partially saturated conditions. Environmental Science & Technology 46, 2633-2641.

Scheinost, A.C. & Sparks, D.L. (2000): Formation of layered single- and double-metal hydroxide precipitates at the mineral/water interface: A multiple-scattering XAFS analysis. Journal of Colloid and Interface Science 223, 167-178.

Thoenen, T., Hummel, W., Berner, U. & Curti, E. (2014): The PSI/Nagra Chemical Thermochemical Database 12/07. PSI Bericht Nr. 14-04. Paul Scherrer Institute, Villigen PSI, Switzerland.

Van Loon, L.R., Baeyens, B. & Bradbury, M.H. (2009): The sorption behaviour of caesium on Opalinus Clay: A comparison between intact and crushed material. Applied Geochemistry 24, 999-1004.

Van Olphen, H. (1963): An introduction to clay colloid chemistry. Interscience Publishers, J. Wiley and Sons. Wiley Subscription Services, Inc., A Wiley Company.

Wick, S., Baeyens, B., Marques Fernandes, M. & Voegelin, A. (2018): Thallium adsorption onto illite. Environmental Science & Technology 52, 571-580.

Appendix A: Experimental details for Ni(II), Co(II), Eu(III) and Th(IV) isotherms for Boda Claystone sample delta-11

Materials

A detailed description on the origin of the Hungarian Boda Claystone formation is given in Breitner et al. (2015). The mineralogical composition of the Boda Claystone sample delta-11 is summarised in Tab. 3-17.

Tracers

The radioisotopes ^{63}Ni, ^{60}Co, ^{152}Eu and ^{228}Th in 0.1 M HCl, purchased from Eckert & Ziegler Isotope Products, Inc. (Valencia, CA, USA), were used in the sorption experiments.

Sorption experiments

The rock samples were ground and sieved in order to obtain crushed rock material with sizes < 63 μm.

Prior to the sorption measurements, the crushed core samples were conditioned to the synthetic Boda Claystone porewater given in Tab. 3-18. The conditioning of the samples with the synthetic porewater was carried out in dialysis bags. The dialysis bags were placed in a 2 L polyethylene flask filled with synthetic porewater and then shaken for 24 hours. After this time, the equilibrated solutions in the flasks were replaced by fresh synthetic porewater and the bottles were again shaken for 24 hours. This procedure was repeated four times. The exact rock content in the final suspensions was determined by heating weighed aliquots for 24 hours at 105 °C and correcting for the salt content. The concentrations of the major elements Na, K, Mg, Ca, Sr, Si and S (SO_4^{2-}) in the liquid phases of the conditioned Boda Claystone batch remained constant during the conditioning procedures and are very similar to the synthetic porewaters (Tab. 3-18).

Sorption isotherms for Ni(II), Co(II), Eu(III) and Th(IV) were measured on delta-11 in its synthetic porewater under atmospheric conditions. Standard solutions covering the required nuclide concentration ranges were prepared in the conditioned synthetic porewaters for each element and were labelled with the corresponding radioisotope. Aliquots of rock suspensions and the appropriately labelled standard solutions were transferred into 40 ml centrifuge tubes and shaken end-over-end for one week. Experimental details (*i.e.* S/L ratio, pH, concentration range) are summarised in Tab. A-1. The phase separation, pH measurements and sampling procedure are the same as described in Section 2.2.1. Aqueous activities were measured using either a Canberra Packard TRI-CARB 2750 TR/LL liquid scintillation counter for ^{63}Ni or a Canberra Packard Cobra Quantum γ-counter for ^{60}Co, ^{152}Eu and ^{228}Th.

Tab. A-1: Summary of the experimental conditions for the sorption isotherms on delta-11

Element	**S:L ratio** [g L^{-1}]	**pH**	**[Me_{eql}] range** [M]
Ni(II)	4.1	7.6 – 8.1	6×10^{-10} – 4×10^{-5}
Co(II)	4.1	7.8 – 8.2	3×10^{-8} – 2×10^{-5}
Eu(III)	1.6	8.0 – 8.1	10^{-11} – 6×10^{-9}
Th(IV)	1.4	7.9 – 8.0	6×10^{-14} – 10^{-10}